Benchmarking of the RAPID Eigenvalue Algorithm Using the ICSBEP Handbook

James Michael Butler, Jr.

Thesis submitted to the faculty of
Virginia Polytechnic Institute and State University
in partial fulfillment of the requirements for the degree of

Master of Science
in
Nuclear Engineering

Alireza Haghighat, Chair
Ranga Pitchumani
Mark Pierson

August 6th, 2019
Falls Church, Virginia

Keywords: neutron transport theory, fission matrix, criticality safety

Benchmarking of the RAPID Eigenvalue Algorithm Using the ICSBEP Handbook

James Michael Butler, Jr.

(ABSTRACT)

The purpose of this thesis is to examine the accuracy of the RAPID (Real-Time Analysis for Particle Transport and In-situ Detection) eigenvalue algorithm based on a few problems from the ICSBEP (International Criticality Safety Benchmark Evaluation Project) Handbook. RAPID is developed based on the MRT (Multi-Stage Response-Function Transport) methodology and it uses the fission matrix (FM) method for performing eigenvalue calculations. RAPID has already been benchmarked based on several real-world problems including spent fuel pools and casks, and reactor cores.

This thesis examines the accuracy of the RAPID eigenvalue algorithm for modeling the physics of problems with unique geometric configurations. Four problems were selected from the ICSBEP Handbook; these problems differ by their unique configurations which can effectively examine the capability of the RAPID code system. For each problem, a reference Serpent Monte Carlo calculation has been performed. Using the same Serpent model in the pRAPID (pre- and post-processing for RAPID) utility code, a series of fixed-source Serpent calculations are performed to determine spatially-dependent FM coefficients. RAPID calculations are performed using these FM coefficients to obtain the axially-dependent, pin-wise fission density distribution and system eigenvalue for each problem. It is demonstrated that the eigenvalues calculated by RAPID and Serpent agree with the experimental data within the given experimental uncertainty. Further, the detailed 3-D pin-wise fission density distribution obtained by RAPID agrees with the reference prediction by Serpent which itself has converged to less than 1% weighted uncertainty. While achieving accurate results, RAPID calculations are significantly faster than the reference Serpent calcu-

lations, with a calculation time speed-up of between 4x and 34x demonstrated in this thesis. In addition to examining the accuracy of the RAPID algorithm, this thesis provides useful information on the use of the FM method for simulation of nuclear systems.

Benchmarking of the RAPID Eigenvalue Algorithm Using the ICSBEP Handbook

James Michael Butler, Jr.

(GENERAL AUDIENCE ABSTRACT)

In the modeling and simulation of nuclear systems, two parameters are of key importance: the system eigenvalue and the fission distribution. The system eigenvalue, known as k_{eff}, is the ratio of neutron production from fission in the current neutron generation compared with the absorption and leakage of neutrons from the system in the previous neutron generation. When this ratio is equal to one, the system is critical and is a self-sustaining chain reaction. Knowledge of the fission distribution is important in the nuclear power industry, as it enables engineers to determine the best reactor core assembly configuration to maintain an even power distribution. Several methods have been developed over the years to effectively solve for a nuclear systems fission distribution and system eigenvalue. Aspects of both Monte Carlo and deterministic transport methods have been combined into RAPID's MRT methodology. It is capable of accurately determining the system eigenvalue and fission distribution in real time.

This thesis examines the accuracy of the RAPID algorithm using four unique problems from the ICSBEP handbook. These problems help us to test the limits of the FM method in RAPID through the modeling of small, unique geometric configurations not seen in large, uniformly configured power reactor cores and spent fuel pools. For comparison, each problem is modeled using the Serpent Monte Carlo code, an accurate code meant to serve as the industry standard for determination of the fission distribution of each problem. This model is then used to generate a set of FM coefficients for use in RAPID calculations. It is demonstrated that the eigenvalues calculated by RAPID and Serpent agree with the experimental data within

the given experimental uncertainty. The fission distribution obtained by RAPID is also in agreement with the Serpent reference model. Finally, the RAPID eigenvalue calculation is significantly faster than the corresponding Serpent reference model, with speed-ups ranging from 4x to 34x demonstrated.

Acknowledgements

I would like to thank my advisor, Dr. Alireza Haghighat, whose guidance and teaching has led me to success in writing this thesis and being successful in my graduate program. I would also like to express my gratitude to the committee, Dr. Ranga Pitchumani and Dr. Mark Pierson, for serving on my committee.

My colleagues have been incredibly important in my learning and in my work. I am grateful to have Ph.D. candidates Valerio Mascolino and Vince Wang for their vast knowledge of everything nuclear engineering, their kindness, and their tolerance of me frequently maxing out our computing cluster. My fellow group members, Jacob Bartel and Quinn Dircks, were paramount in the keeping of my sanity. The three of us went through the whirlwind of becoming simultaneous neutron transport and programming experts together, which proved quite the daunting task. Dr. Nathan Roskoff also deserves a thank you, as his help for the brief month of overlap we had in our programs was almost as essential to the completion of my thesis as his processing code, pRAPID.

I am thankful for my parents, Jim and Tammy Butler, for their unwavering support and encouragement throughout my academic career and in my life as a whole. Finally, I am beyond grateful to my girlfriend, Mary Kate Appel. She chose to move to Blacksburg, a town completely foreign to her, to be with me during my first year of graduate school. Since then, she has shown me nothing but love and support while away in Charlottesville establishing her professional career in marketing.

Contents

List of Figures

List of Tables

Chapter 1

Introduction and Background

1.1 Introduction

The simulation of neutronics is an important aspect in the modeling of nuclear systems, but is complex and requires sophisticated computational methods to obtain accurate results. Eigenvalue calculations are essential for the determination of the criticality eigenvalue and the fission distribution. There are deterministic, Monte Carlo, and hybrid methods for performing eigenvalue calculations, each with pros and cons. Deterministic calculations are generally performed for obtaining detailed solutions, however the amount of detail is constrained by the problem size and memory available. Monte Carlo methods are good for obtaining reference solutions as they are capable of defining exact geometries and using continuous-energy cross-sections, and do not require as much memory. However, eigenvalue Monte Carlo calculations are faced with uncertainties from poor source convergence and cycle-to-cycle correlations, issues that result in long calculation times by the computer and long work times for the analyst [3]. In some situations, the calculation may never converge.

Monte Carlo methods are discussed more in detail in section 2.2. In this thesis,

the accuracy of the hybrid RAPID code system is examined using four benchmark problems from the ICSBEP handbook. The first problem is a critical approach experiment using three clusters of fuel rods in a pool of water. The second problem is similar to the first, with the inclusion of reflecting walls along the geometry and absorbing plates outside the central cluster. The third is a critical moderator height experiment consisting of four fuel assemblies each surrounded by a strong cadmium absorbing canister. The final benchmark problem studied is a simplified model of a particular core configuration of the IPEN/MB-01 research reactor. For each benchmark problem, a Monte Carlo reference calculation is performed using the Serpent Monte Carlo code [5]. A chapter is dedicated to the results and examination of each benchmark problem.

The RAPID code system is typically used to model large systems, particularly spent fuel pools, casks, and reactor cores [12]. For these calculations, RAPID benefits from existing similarities and symmetries. Additionally, it can use novel axial translation techniques. These techniques significantly simplify generation of the fission matrix coefficients. However, in this thesis, the models benchmarked are small, unique in geometry, and use fresh, low enriched fuel. Studying these models will help to learn about the limitation of RAPID's approach in generating fission matrix coefficients, as the benchmark problems differ in size, geometric similarity, and symmetry.

Fission matrix coefficients are calculated for each benchmark problem for use in RAPID's fission matrix algorithm. These results are compared with experimental values and with reference eigenvalue Monte Carlo calculations performed in Serpent. For both calculations there are uncertainties in the tallied regions. In the reference eigenvalue Monte Carlo calculation, care must be taken in the selection of run parameters to avoid as much undersampling as possible. However, in the FM coefficient calculation, the uncertainty can be reduced by increasing the number of particles used.

To make the modeling of the selected benchmark problems with RAPID possible, the source code for RAPID has been generalized to properly handle arbitrary rectangular geometries. The pre- and post-processing code utilized by the Virginia Tech Transport Theory Group (VT^3G), pRAPID, has been modified to handle arbitrary rectangular geometries in fresh fuel scenarios, which encompasses all four of the benchmark problems examined in this thesis. The detailed changes to pRAPID have been documented in appendix C.

Organization of Thesis

This thesis starts by giving a discussion of the theory necessary to understand RAPID and the MRT methodology, which itself is then described after the theory section. Then, a description of the pRAPID utility code used for input preparation and processing of RAPID models is given. Next, an introduction to each of the four benchmark problems is given in section 4.1.

From there, a source convergence study is performed to determine appropriate convergence criteria for reference Monte Carlo calculations, and how to select run parameters based on those criteria. This allows for a consistent comparison between RAPID models and their Monte Carlo counterpart. This is followed up by a chapter of results and analysis for each benchmark problem studied. Finally, a summary of results from all four benchmark problems is given containing eigenvalue results and calculation speed-ups, with conclusions and future work shown at the end.

Chapter 2

Theory

This chapter describes the theory behind the methods used in this thesis. It talks about the linear Boltzmann transport equation and gives an introduction to the different neutron transport computational methods that are relevant to this work. This chapter gives the background information necessary to discuss the RAPID methodology in more detail.

2.1 The Linear Boltzmann Equation

The time-independent form of the linear Boltzmann Equation (LBE) is a particle balance equation used in neutron transport [6]. The time-independent form of the LBE is used for design and analysis of nuclear systems at steady-state conditions. The general time-independent LBE is given in equation 2.1.

$$[\hat{\Omega}\cdot\vec{\nabla}+\sigma(\vec{r},E)]\Psi(\vec{r},\hat{\Omega},E)] = \int dE' \int d\Omega' \sigma_s(\vec{r},E'\rightarrow E,\hat{\Omega}'\cdot\hat{\Omega})\Psi(\vec{r},E',\hat{\Omega}') + \frac{\chi(E)}{4\pi}\int dE'\nu\sigma_f(\vec{r},E')\int d\Omega'\Psi(\vec{r},E',\hat{\Omega}')+q_{ex}(\vec{r},\hat{\Omega},E) \quad (2.1)$$

Overall, equation 2.1 can be thought of as the balance of gains and losses of neutrons in the phase space ($d^3rdEd\Omega$).

On the left hand side, $(\hat{\Omega} \cdot \vec{\nabla})\Psi(\vec{r}, \hat{\Omega}, E)$ represents the flow of neutrons without interaction from the phase space due to streaming in and out of the phase space ($d^3rdEd\Omega$). The other term, $\sigma(\vec{r}, E)\Psi(\vec{r}, \hat{\Omega}, E)$, represents the loss of neutrons from the phase space due to particle interactions.

On the right hand side of equation 2.1, the three terms represent the sources of gains of neutrons in the phase space. The first term, $\int dE' \int d\Omega' \sigma_s(\vec{r}, E' \rightarrow E, \hat{\Omega}' \cdot \hat{\Omega})\Psi(\vec{r}, E', \hat{\Omega}')$ represents the scattering of neutrons with energy *E'* traveling in direction $\hat{\Omega}'$ into energy *E* and direction $\hat{\Omega}$. In this case, the first term refers to down-scattering of neutrons from energy *E'* to energy *E*. This term is also represented by neutrons scattering from one direction $\hat{\Omega}'$ into the direction $\hat{\Omega}$ defined by the phase space.

The second term, $\frac{\chi(E)}{4\pi} \int dE' \nu\sigma_f(\vec{r}, E') \int d\Omega' \Psi(\vec{r}, E', \hat{\Omega}')$, is the fission term. This represents the gain of neutrons in the phase space born through fission. $\chi(E)$ is the fission spectrum, which dictates the the energy distribution of fission neutrons. The third term, $q_{ex}(\vec{r}, \hat{\Omega}, E)$, represents the contribution of neutrons to the system through external sources in the phase space.

2.2 Monte Carlo Transport Methods

The Monte Carlo method is a stochastic approach for finding solutions to the LBE for a given system. It has grown in popularity with the advent of high performance parallel computers coupled with the development of advanced codes. Rather than explicitly solving the LBE through discretization of space, energy, and directions of the system, Monte Carlo methods sample a large number of particle histories according to probability distributions modeling neutron behavior. Monte Carlo methods

typically follow the law of large numbers, which is a theorem that states that performing the same experiment multiple times averages out the expected result. In any statistical method, an increase in the amount of data reduces the uncertainty on the average quantity.

2.2.1 Eigenvalue Monte Carlo

Most fundamental physical interactions are guided by some random process, with the capability to be measured to some sort of average value. In terms of Monte Carlo transport, typical random processes derive from particle interactions (fission, scattering, and absorption). These random events follow a given probability density function. Eigenvalue Monte Carlo codes such as Serpent [5] and MCNP [13] start a simulation by guessing the source distribution, and then transporting each source particle until it is absorbed or escapes from the system. If the absorption leads to a fission process, then the subsequently created fission neutrons represent the source for a new generation of cycle. This procedure is repeated until a precise eigenvalue and/or fission density distribution is achieved within a a given tolerance. Since the source is unknown, the eigenvalue Monte Carlo method requires used defined parameters including number of particles per cycle and the number of skipped cycles. Additionally, to obtain a precise solution, the number of active cycles has to be provided by the user. All of these are problem dependent, and have to studied for any new problem. The number of particles per cycle improve the statistics of the calculation within each cycle, while the number of active cycles increase the number of estimates of k_{eff} and the source distribution obtained, which decreases the uncertainty on those estimates. Like all methods, there are trade-offs between computation time and desired precision. Using too few particles per cycle or too few skipped cycles can lead to an unconverged fission source or underestimated eigenvalue. These problems were rampant in early stages of Monte Carlo code development due to computers

not being able to handle the memory load necessary for a converged solution. This was clearly demonstrated by Elliot Whitesides with the "Criticality of the World" problem [14].

2.3 Criticality Problems and the Fission Matrix Method

This section discusses modifications to the LBE used by Monte Carlo codes to solve the transport equation to determine the criticality of a system. Then, the fission matrix (FM) method and the approach used in the RAPID code system to obtain the fission matrix coefficients will be discussed.

2.3.1 Criticality Problems

To start, equation 2.1 must be converted from the time-independent fixed source form to an eigenvalue form via the introduction of the eigenvalue k [4].

$$[\hat{\Omega}\cdot\vec{\nabla}+\sigma(\vec{r},E)]\Psi(\vec{r},\hat{\Omega},E)] = \int dE' \int d\Omega'\sigma_s(\vec{r},E'\rightarrow E,\hat{\Omega}'\cdot\hat{\Omega})\Psi(\vec{r},E',\hat{\Omega}') + \frac{\chi(E)}{4\pi k}\int dE'\nu\sigma_f(\vec{r},E')\int d\Omega'\Psi(\vec{r},E',\hat{\Omega}') \quad (2.2)$$

Where the q_{ex} term has been removed, as it is negligible compared to the fission neutrons. To derive the fission matrix form of the LBE, the equation is written in an operator form as:

$$H\Psi(\vec{r},\hat{\Omega},E) = \frac{1}{k}F\Psi(\vec{r},\hat{\Omega},E) \quad (2.3)$$

Where the fission operator F is defined as:

$$F = \frac{\chi(E)}{4\pi} \int_0^\infty dE' \int_{4\pi} d\hat{\Omega}' \nu\sigma_f(\vec{r}, E') \tag{2.4}$$

and the transport operator H is defined as:

$$H = \hat{\Omega} \cdot \vec{\nabla} + \sigma(\vec{r}, E) - \int_0^\infty dE' \int_{4\pi} d\hat{\Omega}\sigma_s(\vec{r}, E' \to E, \hat{\Omega}' \cdot \hat{\Omega}) \tag{2.5}$$

Where $\Psi(\vec{r}, \hat{\Omega}, E)$ is the angular flux at position $\vec{r}$ within d^3r, direction $\hat{\Omega}$ in solid angle $d\Omega$, and energy E within dE.

2.3.2 The Fission Matrix Method

To start, the fission spectrum χ can be removed from the fission operator, such that the operator form of the LBE becomes:

$$H\Psi(\vec{r}, \hat{\Omega}, E) = \frac{1}{k}\chi\tilde{F}\Psi(\vec{r}, \hat{\Omega}, E) \tag{2.6}$$

Ψ is obtained by re-arranging terms over to the right side:

$$\Psi = \frac{1}{k}H^{-1}\chi\tilde{F}\Psi \tag{2.7}$$

If both sides are multiplied by $\tilde{F}$, the terms can be grouped again to give a better representation of what the operators represent:

$$\tilde{F}\Psi = \frac{1}{k}(\tilde{F}H^{-1}\chi)\tilde{F}\Psi \tag{2.8}$$

Which can be written as the eigenvalue formulation which is used to determine k and the source distribution:

$$\mathbf{S} = \frac{1}{k}\underline{\underline{\mathbf{A}}}\mathbf{S} \tag{2.9}$$

Where $\mathbf{S} = \tilde{F}\Psi$ and $\underline{\underline{\mathbf{A}}} = \tilde{F}H^{-1}\chi$. $\mathbf{S}$ represents the fission source, and $\underline{\underline{\mathbf{A}}}$ represents the continuous form of the fission matrix.

Note that the calculation of FM coefficients is unique, using a fixed-source Monte Carlo approach in their generation. This method will be explained in detail in the following chapter.

Chapter 3

RAPID and the MRT Methodology

3.1 RAPID Introduction

RAPID is a hybrid-method transport code capable of quickly and accurately determining the criticality eigenvalue k_{eff}, sub-critical multiplication eigenvalue M, 3D fission source distributions, as well as detector response for a given model. It calculates the two eigenvalues using the fission matrix method, after sets of FM coefficient calculations (via fixed-source Monte Carlo models) are performed. Any Monte Carlo transport code providing accurate FM coefficients may be used. However, pRAPID is designed to generate and process FM coefficients using the Serpent Monte Carlo transport code [5].

FM coefficient sets can be calculated using multiple types of assemblies which can vary in materials and burn-up. The techniques used by RAPID to take advantage of geometric similarities will be discussed, as they are essential to RAPID's near real-time modeling capability in reactor cores and spent fuel pools. However, in this

thesis these techniques are shown to not be effective given the small system size and unique geometries of the benchmark models chosen, with the only symmetry available being quarter symmetry.

Depending on the geometric symmetries and similarities available, RAPID is capable of near real-time analysis in terms of fission source distribution and criticality eigenvalue. Near real-time is defined as being in the seconds to a few minutes needed for a full calculation. This can be potentially be up to 1,000 times faster [12] than traditional eigenvalue Monte Carlo methods. The other important aspect to RAPID besides the calculation speed-up is that, depending on the types of assemblies and burn-up steps used, assemblies can be re-arranged and the eigenvalue calculation can be re-run to determine k_{eff} and the source. This can be particularly useful in the analysis of reactor core assembly loadings and spent fuel pool assembly organization. This is done by keeping the fission matrix calculation separate from the fission matrix coefficient pre-calculations, in what is defined as the MRT methodology.

3.2 MRT Methodology

The MRT methodology utilized by RAPID for models not involving burn-up follows a two step process. The first step is to generate FM coefficients as described in section 2.3.2 using a set of fixed source Monte Carlo calculations in Serpent. This means tallying for fission neutron production across the fuel model, and then either define the source location using a full FM approach or some sort of symmetry, dependent on model geometry. In all cases presented in this thesis, either a full FM calculation was necessary, or quarter symmetry could be used. Geometric similarities will typically lead to nearly identical FM coefficients, which is an approach heavily used by RAPID through mapping of coefficients elsewhere in the model dependent on geometry, which greatly reduces the number of FM coefficients needed to accurately characterize

the model. This mapping of coefficients provides a significant calculation speedup through the reduction of FM coefficients needed, but also in the reduction of the fission matrix size.

Figure 3.1 shows the multiple stages of the MRT methodology utilized by RAPID. As described before, this thesis only utilizes the fission matrix coefficient calculations in cases of fresh fuel, and does not need to utilize the bRAPID algorithm[10].

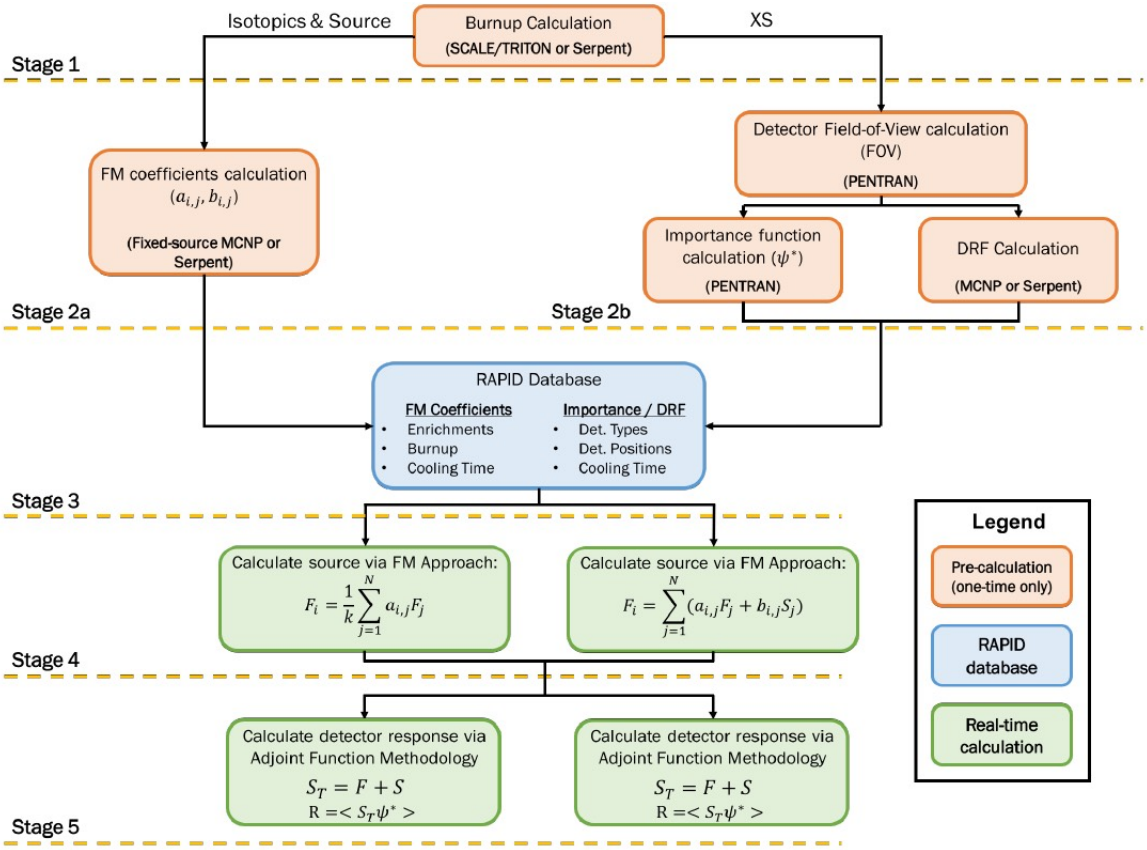

Figure 3.1: RAPID Methodology Flowchart

3.2.1 pRAPID

pRAPID, also known as Pre- and Post-processing for RAPID, is an input preparation utility code developed to be the workhorse for RAPID. It is capable of automatically generating all input files necessary to build a RAPID or bRAPID model, handling both pre-calculations and the processing of them afterwards. pRAPID and RAPID share the responsibility of filling the fission matrix for a given problem, and take advantage of geometric similarities, symmetries, axial translation, and boundary correction techniques to reduce the amount of information needed to fill in the entire fission matrix. These four techniques are briefly described below, however only the symmetry technique is used for the benchmark problems described in this thesis.

The first stage of the methodology, FM coefficient calculation, involves a set of N fixed-source Serpent calculations for each burnup step and power density, where N is user-defined and model-dependent. In the RAPID calculations done in this thesis, the coefficient calculations consisted of pin-wise sources, each about one inch in height. However, increasing the height of the source was explored through fission matrix collapsing in section 7.3.2. For each fission region j, a mesh tally is defined over N defined fuel regions to measure the number of fission neutrons produced in region i per unit source of region j. These FM coefficients were defined in equation 3.4. To get a better idea of how these coefficient calculations are performed, see figure 3.2. Here, the source is located in the red region and transported throughout the model, while a tally in each fuel region is performed to determine the number of fission neutrons produced. Moving the source to each location leads to the generation of FM coefficients.

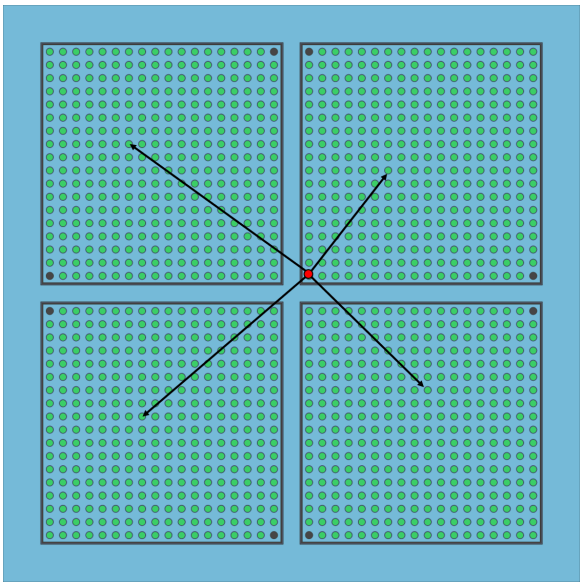

Figure 3.2: Depiction of FM Coefficient Calculation

In models containing geometric similarities and symmetries, such as the model shown in figure 3.2, a detailed, accurate calculation can be made using only a small fraction of the FM coefficients. In benchmark problem 3, described in detail in section 4.2.3, quarter symmetry was used to reduce the number of FM coefficients needed for a full calculation from 46,656 to 11,664. One of the processing routines implemented in pRAPID was modified to do this symmetric flipping to build the full fission matrix. The processing routine would take the source and tally information calculated in figure 3.2 and project it as shown in figure 3.3.

This was the extent of FM coefficient mapping used by the benchmark models presented in this thesis. However, to give a better description of how geometric similarities can be leveraged in this way, a closer look can be taken at the GBC-32 computational benchmarking work done by current group member and Ph.D. candidate Valerio Mascolino [7][8]. The GBC-32 dry storage cask consists of a type 304 stainless steel cylindrical canister, holding 32 pressurized water reactor (PWR) fuel

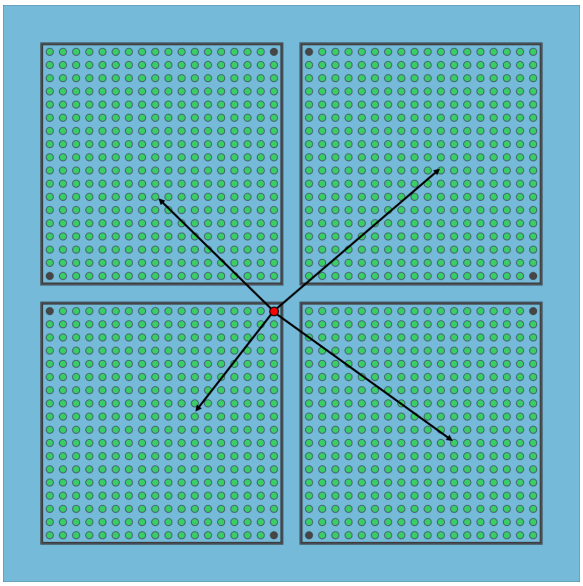

Figure 3.3: Source and Tally Info Mapped from Top-Right to Bottom-Left

assemblies each consisting of 17x17 fuel rods, each with an active height of 365.76 cm. Serpent geometric plots for this cask are shown in figures 3.4 and 3.5. For the sake of simplicity, the benchmarking started with filling this cask with fresh UO_2 fuel enriched to 4 wt.% ^{235}U. Without geometric similarity, this would be impossible to model appropriately, since $N * N = (32 * 264 * 24)^2 = 4.1 * 10^{10}$ fission matrix elements would need to be calculated. However, PWR fuel is built to be largely symmetric both radially and axially to achieve a smooth flux profile in a PWR core.

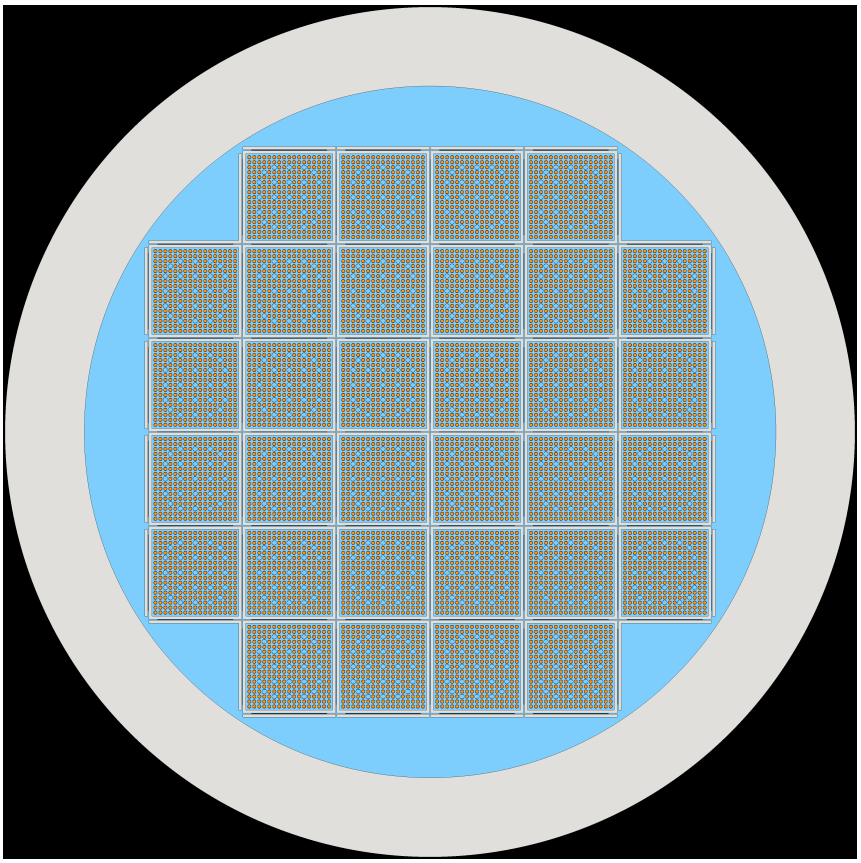

Figure 3.4: X-Y View of the GBC-32 Cask

In this model, each assembly can take advantage of octal symmetry, only needing coefficients to be calculated in the triangular region shown in figure 3.6. This model takes advantage of octal symmetry, coefficient mapping, and an axial translation scheme to further reduce computation time.

Geometric Similarity and ROI

In systems with geometric similarities at the assembly level, the FM coefficients can be mapped to the surrounding assemblies, as the behavior is largely the same until an axial or radial boundary assembly is reached, which then may or may not necessitate a boundary correction. In the case of the GBC-32 cask, absorbers surrounding

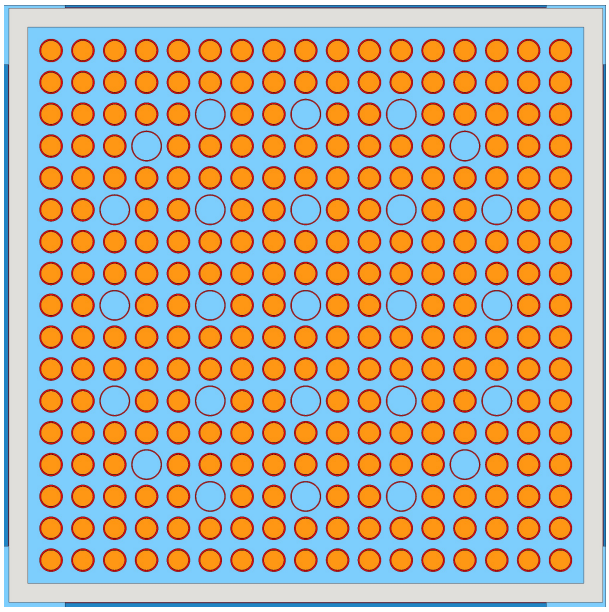

Figure 3.5: 17x17 Assembly in GBC-32 Cask

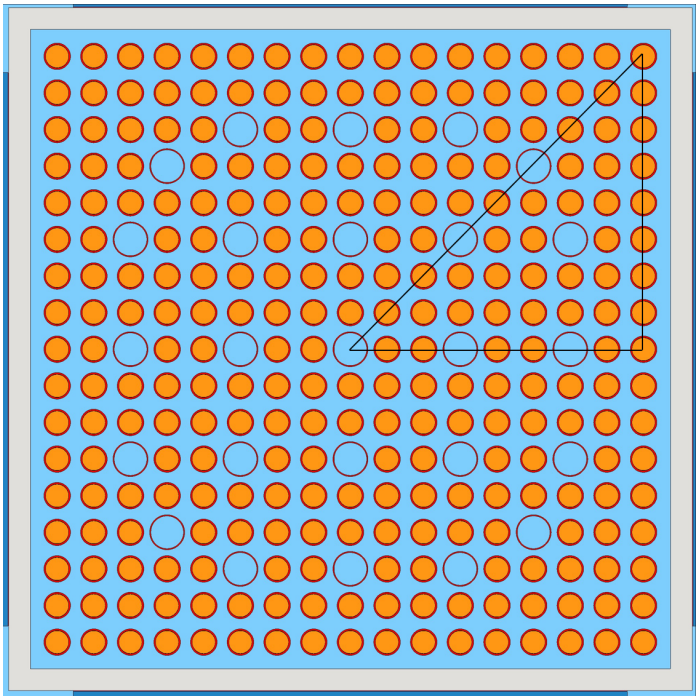

Figure 3.6: Octal Symmetry Example for FM Coefficient Calculation

the assemblies effectively decouples the assemblies, thus eliminating the need for a boundary correction. The boundary correction methodology is discussed in detail in section 6.2.1. Regardless, the central assembly's coefficients are able to be mapped to all other assemblies in the cask, as shown in figure 3.7b. A radial region of importance (ROI) can be defined, depending on the problem. This region should contain a majority (99%) of the total fission production in the model, which in a spent fuel cask is typically about two assemblies away radially [10]. Determining this ROI allows us to ignore tallies outside this region, further reducing the amount of calculation needed to fill in the fission matrix. In this problem, the ROI contained the two rings of assemblies outside of the central one, defined in RAPID as the number of relative assemblies (NAR) [11] being equal to 2.

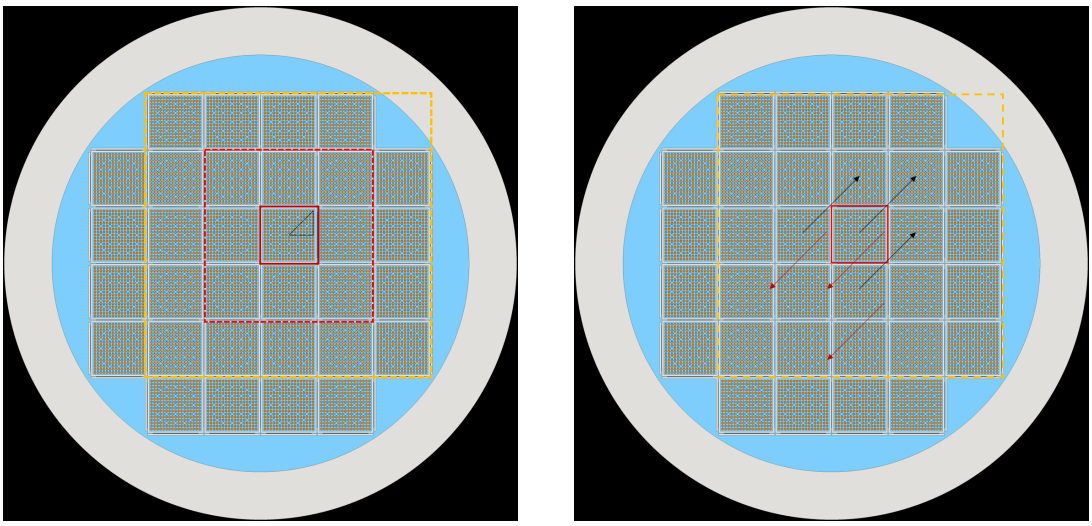

(a) Region of Importance (b) FM Coefficient Mapping

Figure 3.7: GBC-32 Region of Importance and FM Coefficient Mapping

Axial Translation

The axial translation scheme technique by RAPID needs to be discussed, as it is used in the first two benchmark problems, but it was demonstrated that it is not effective. In terms of axial behavior, the magnitude of fission is symmetric, and is largely uniform except near the top and bottom boundaries. Like the radial ROI, an axial ROI can also be obtained by defining the region encompassing most of the fission due to a source located in the center of the model. This is depicted by the dashed box in figure 3.8.

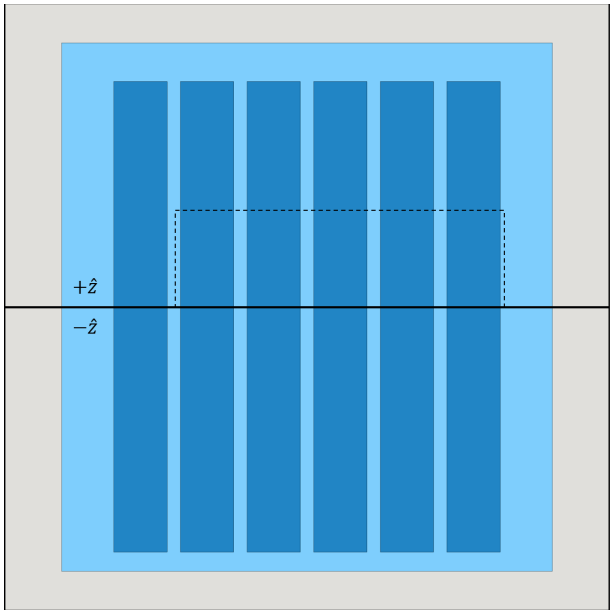

Figure 3.8: Axial Region of Interest for GBC-32

Figures 3.9 and 3.10 depict a generic fuel pin [10]. They show how FM coefficient data is tallied from the center up, reflected below, and then translated up and down the model to fill in the fission matrix. Thus, the octal symmetry, coefficient mapping, and axial translation allow for large systems such as a PWR core to be accurately modeled using only one octant of one central assembly, while also reducing the number of pre-calculations necessary.

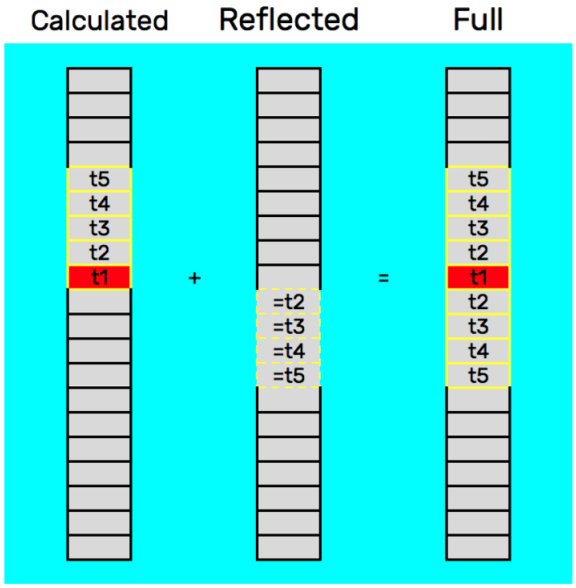

Figure 3.9: Demonstration of the Reflection of FM Coefficients from the $+\hat{z}$ Direction to the $-\hat{z}$ Direction

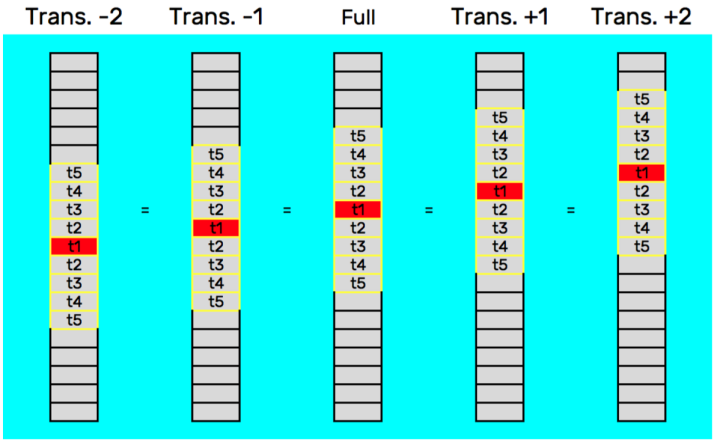

Figure 3.10: Axial Translation of FM Coefficients

Boundary Correction

The last technique used in FM coefficient calculation is the boundary correction methodology. The purpose of boundary correction is to correct the fission matrix coefficients. This is done by performing two calculations for a flat source distribution; one with reflective boundary conditions, and one with correct boundary conditions. The fission neutron production rate is tallied pin-wise over the reference geometry portions of each model and a ratio is taken.

$$bnd(x, y, z) = \frac{f_{ref}(x, y, z)}{f_{inf}(x, y, z)} \tag{3.1}$$

Equation 3.1 is applied to the coefficients.

$$a_{i,j} = bnd(x_i, y_i)\tilde{a}_{i,j} \tag{3.2}$$

Where $\tilde{a}_(i, j)$ is the uncorrected fission matrix coefficient.

3.2.2 RAPID Power Iteration

To determine the fission source distribution and the eigenvalue, equation 3.3 is solved:

$$S_i = \frac{1}{k} \sum_{j=1}^{N} a_{i,j} S_j \tag{3.3}$$

Where the fission matrix coefficients, $a_{i,j}$, are defined as:

$$a_{i,j} = \frac{\int_{V_i} d^3r \int_{V_j} d^3r' a(\vec{r}' \rightarrow \vec{r}) S(\vec{r}')}{\int_{V_j} d^3r' S(\vec{r}')} \tag{3.4}$$

Which represents the number of fission neutrons produced in cell i due to fission neutrons born in cell j.

This equation is solved using the power iteration technique. The convergence criteria uses relative difference in both fission source and eigenvalue, and are set to 10^{-5} and 10^{-6}, respectively. The algorithm below shows the skeleton code of the RAPID power iteration process [11].

Algorithm: RAPID Power Iteration Method

Initialize Variables

Source: $S_i^{(0)}$

Eigenvalue: $k^{(0)}$

Source Tolerance: ϵ_S

Eigenvalue Tolerance: ϵ_k

Max Iterations: N_k

Perform Iteration

while $n \leq N_k$ **do**

$n = n + 1$

$S_i^{(n)} = \frac{1}{k^{(n-1)}} \sum_j a_{i,j} S_j^{(n-1)}$

$k^{(n)} = \frac{\sum_i S_i^{(n)}}{\sum_i S_i^{(n-1)}}$

$\Delta_{S_i} = \frac{S_i^{(n)} - S_i^{(n-1)}}{S_i^{(n-1)}}$

$\Delta_k = \frac{k^{(n)} - k^{(n-1)}}{k^{(n-1)}}$

if $max(\Delta_{S_i}) < \epsilon_S$ & $\Delta_k < \epsilon_k$ **then**

return $S_i^{(n)}, k^{(n)}$

exit()

end

end

Chapter 4

Benchmark Problems

4.1 ICSBEP and Selected Benchmarks

In 1992, the Criticality Safety Benchmark Evaluation Project (CSBEP) was initiated by the U.S. Department of Energy (DOE) under direction of the Idaho National Engineering and Environmental Laboratory. In 1995, the CSBEP became an official activity of the NEA Nuclear Science Committee, which then renamed the project to the ICSBEP. The ICSBEP Working Group was tasked with the main goal of compiling critical and sub-critical benchmark experiments into a standard format for nuclear engineers to have a comprehensive tool to validate their calculation tools and cross-section libraries. The ICSBEP has grown significantly from the original scope of the work, from 406 cases in 1995 to 4,874 cases documented in 2015 [2].

The ICSBEP handbook is split up and categorized by fissile media, physical form of the fissile material, and neutron energy range. Since RAPID was designed for simulation of spent fuel pools and reactor cores, all of my benchmark models were selected from the "LEU-COMP-THERM" section of the handbook. This refers to low enriched uranium (LEU), compound fuel materials (COMP), and a thermal fis-

sion spectrum (THERM). In each benchmark problem in the handbook, the original experiment is described in detail, and sensitivity studies are performed to simplify the model down to an easily reproducible computational benchmark model. For each benchmark problem, the handbook provides a benchmark k_{eff} and an estimate of the experimental uncertainty. Also typically provided are several quick reference calculations to verify that the benchmark problem created is acceptable for use elsewhere. These were particularly easy to read through in order to get an idea of what the purpose of the original experiment was. The documentation for the geometry was very precise, which allowed for creation of Serpent reference models using the provided geometry. Using a more modern Monte Carlo code, along with modern cross-section libraries led to accurate reference models upon which to base RAPID calculations. To simplify labeling of figures, each benchmark problem is labeled in the order they are presented as Benchmark Problem 1, Benchmark Problem 2, etc.

4.2 Selected Benchmarks

4.2.1 Benchmark Problem 1: LEU-COMP-THERM-001

Introduction

This experiment was a critical approach experiment performed at the Critical Mass Laboratory at the Pacific Northwest National Laboratories. The title of the experiment is *Water-Moderated UO_2 (2.35%) Fuel Rods in 2.032 cm Square-Pitched Arrays*. It consisted of eight cases, varying the number of fuel rods per cluster. These cases were tested at room temperature, in an open-topped carbon-steel tank filled with light water. Case 1 of this experiment consisted of one cluster of UO_2 fuel rods. This served to determine how many rods were needed to achieve criticality given the rod dimensions, enrichment, and pitch. The remaining seven cases consisted of three rectangular clusters of varied numbers of fuel rods. Figure 4.1 shows the cluster geometries and associated critical separations. The first model benchmarked in RAPID was case 7 of this experiment. The case 7 cluster geometry consisted of 280 (20x14) fuel rods each, with a critical cluster spacing of 4.46 cm. This model served as a good example of a rectangular geometry previously not tested by the RAPID source code, and to test whether RAPID's axial translation algorithm is effective with relatively short fuel heights seen in these small benchmark problems.

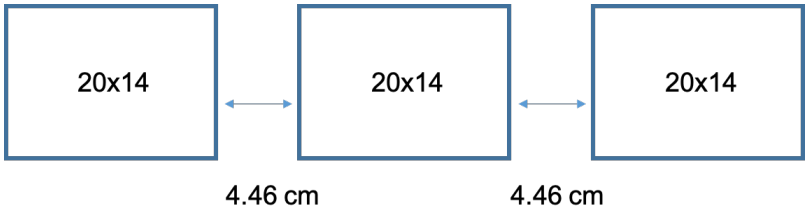

Figure 4.1: Critical Cluster Configuration for Benchmark Problem 1

Benchmark Specifications

Since the point of the ICSBEP was to create experimental benchmark problems for use in industry and academia, simplifications to the actual experiments were made based on sensitivity studies performed for each experiment. Typically, these simplifications removed most structural materials as they typically had a trivial contribution to the criticality calculation. For this benchmark problem, only the fuel rods, the water, and the lower reflector plate were considered. The acrylic lattice plates holding the rods together were also removed, despite having a non-trivial (0.02%) effect on k_{eff}. The result of removing these lattice plates was factored into the estimated benchmark k_{eff}.

The fuel rods consisted of UO_2 pellets with an enrichment of 2.35 wt.% ^{235}U, in a type 6061 aluminum cladding, with an active fuel height of 91.44 cm. The top plug of the fuel rods consisted of type 1100 aluminum, with the corresponding bottom plug consisting of type 5052 aluminum. Figure 4.2 shows the schematic of the fuel rods used in this experiment. The fuel clusters were placed on an acrylic support plate, which also served as a reflector plate.

Since the reported experimental configurations were extrapolations to a critical separation, the benchmark k_{eff} was given as 1.000. However, due to the effects on k_{eff} from the lattice plates, the effect was subtracted, leading to a final benchmark $k_{eff} = 0.99800 \pm 0.00310$. The uncertainty on k_{eff} was determined through sensitivity studies relating to uncertainty in fuel rod properties, cluster separation distance, water temperature, and water impurities.

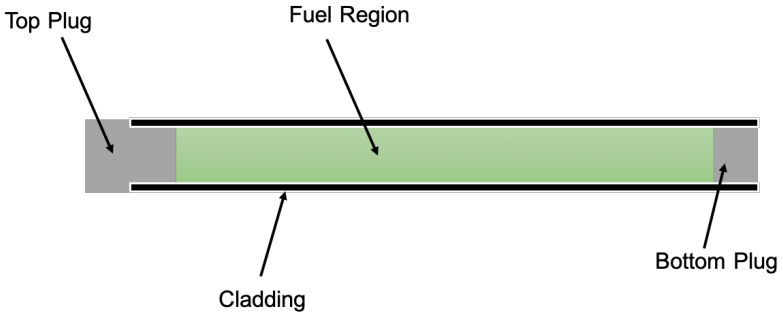

Figure 4.2: Fuel Rod Schematic for Benchmark Problem 1

4.2.2 Benchmark Problem 2: LEU-COMP-THERM-013

Introduction

This experiment was another critical approach experiment at the Critical Mass Laboratory at the Pacific Northwest National Laboratories. While LEU-COMP-THERM-001 simply consisted of UO_2 fuel rods in water atop a reflector plate, this experiment incorporated the use of steel reflecting walls, and included varying absorber plate materials up against the central assembly. The title of this experiment is *Water-Moderated Rectangular Clusters of UO_2 (4.31%) Fuel Rods (1.892 cm Pitch) Separated by Steel, Boral, Boroflex, Cadmium, or Copper Plates, with Steel Reflecting Walls*. Figure 4.3 shows the general X-Y view of this benchmark problem.

There were seven cases tested in this experiment, where absorber plate material was varied. Critical cluster separation was the desired measurement. All seven cases had three clusters of 192 (12x16) fuel rods each. Figure 4.4 shows the absorber material, absorber thickness, as well as the critical separation distance, denoted as S_C for each case. Case 1 from this experiment was selected for detailed examination. This benchmark problem is useful because it allows us to test and compare the RAPID algorithm in a small system that is more decoupled than the previous model.

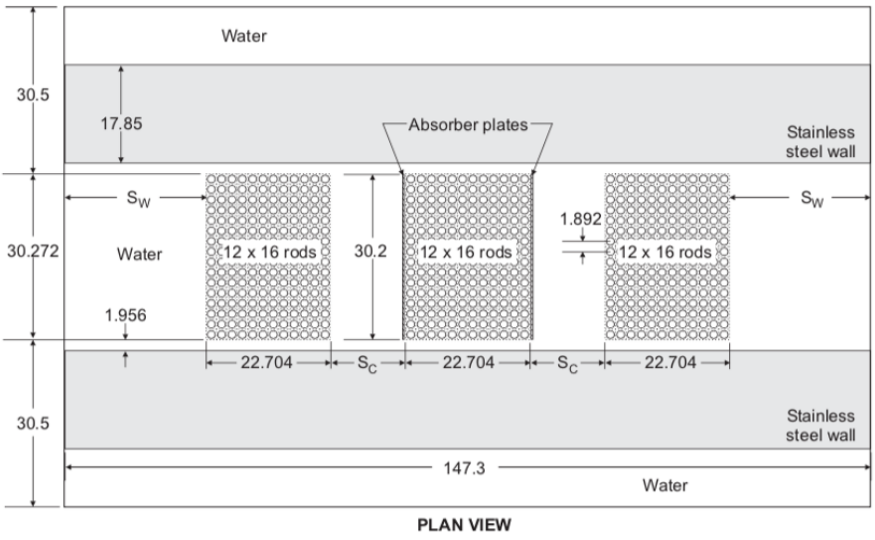

Figure 4.3: Plan View for Benchmark Problem 2 Geometry [1]

Case	Separation of Clusters, S_c (cm) [(a)]	Absorber-Plate Material	Absorber-Plate Thickness (cm)
1	13.273	304-L Steel	0.302
2	9.353	304-L Steel with 1.1 wt.% B	0.298
3	7.823	Boral B	0.216[(b)]
4	7.893	Boroflex	0.226[(c)]
5	8.463	Cadmium	0.061[(d)]
6	12.993	Copper	0.337
7	10.093	Copper-Cadmium	0.357

(a) Distance between outer cell boundaries of one cluster and outer cell boundaries of the next. This distance is (pitch – rod diameter) = 0.477 cm less than rod-surface-to-rod-surface separation of clusters in Table 2.
(b) Also 0.038 cm of Type 1100 aluminum on either side of the 0.216-cm-thick B_4C-Al absorber material.
(c) Also 0.16-cm-thick Plexiglas on either side of the 0.226-cm-thick Boroflex.
(d) The 0.061-cm-thick cadmium is mounted on 0.296-cm-thick Plexiglas, with the cadmium next to the center cluster.

Figure 4.4: Critical Configurations for Benchmark Problem 2 [1]

Benchmark Specifications

This benchmark model was created from the experiment in a similar fashion to LEU-COMP-THERM-001. All structural materials were removed, except for the lower

reflector plate, absorber plates, and steel reflecting walls. These simplifications were made using the results from sensitivity studies performed by the experiment reviewer. The lattice plates were removed despite their non-trivial effect (0.02%) on k_{eff}. This contribution is reflected in the uncertainty of the benchmark model k_{eff}. This differs from benchmark problem 1, where the effect on k_{eff} due to the lattice plates was subtracted from the benchmark k_{eff}.

The fuel rods in this experiment were axially symmetric in their geometry. They consisted of UO_2 pellets enriched to 4.31 wt.% ^{235}U, in a type 6061 aluminum cladding plugged on each end with a 2.2225 cm long rubber end plug. The fuel rod dimensions are shown in figure 4.5. The case 1 absorber material was type 304-L stainless steel, with a thickness of 0.302 cm, and leading to a critical separation distance of 13.273 cm between the clusters.

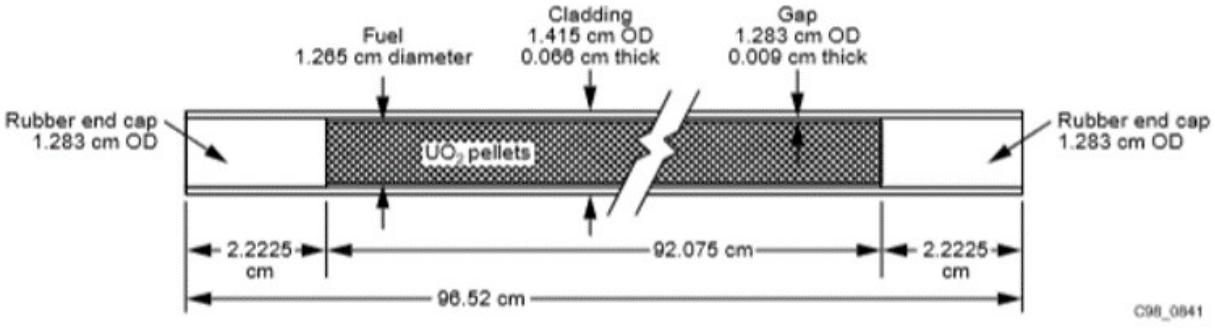

Figure 4.5: Fuel Rod Schematic for Benchmark Problem 2 [1]

The benchmark k_{eff} for case 1 was determined to be $k_{eff} = 1.00000 \pm 0.00180$. The uncertainty was determined through sensitivity studies performed by the reviewers and was largely related to uncertainty in fuel rod characterization, absorber plate characterization, separation uncertainties between clusters, and distance from the reflecting walls. The plan and elevation views of the benchmark specification are obtained from this experiment's review document and are shown in figures 4.3 and

4.6, respectively.

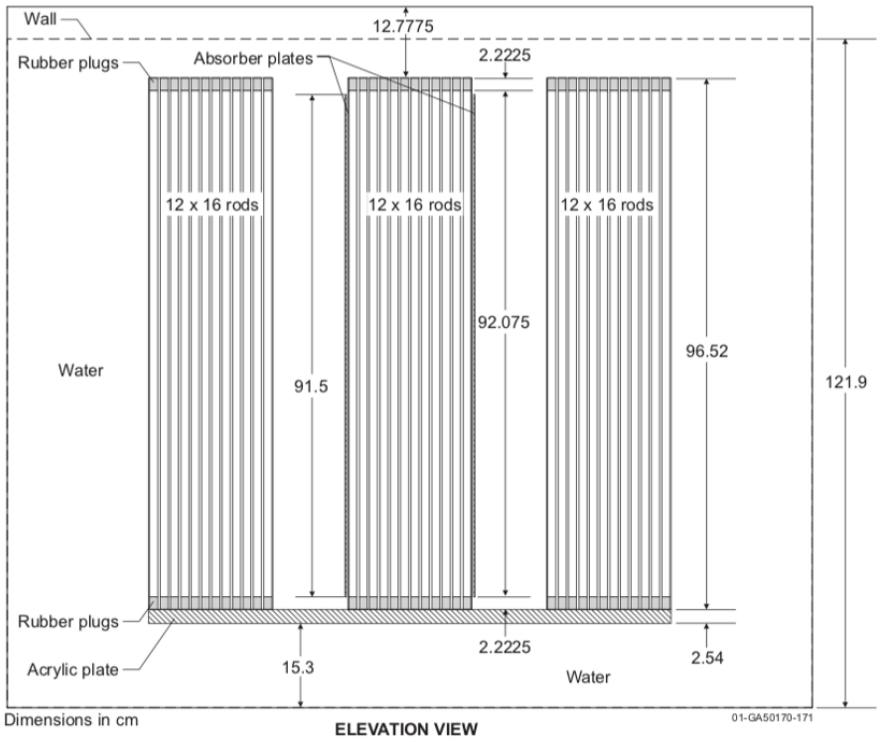

Figure 4.6: Elevation View for Benchmark Problem 2 Geometry [1]

4.2.3 Benchmark Problem 3: LEU-COMP-THERM-034

Introduction

LEU-COMP-THERM-034 was different compared to the previous two experiments discussed. While the other two were critical approach experiments, this was a critical moderator height experiment. This series of moderator height experiments took place at the experimental criticality facility at the French Alternative Energies and Atomic Energy Commission. The experiment's tank was filled with water until a near-critical state was reached. The critical moderator heights were then extrapolated to critical, where the experimenters stopped 0.1% away from a multiplication factor of 1.000. Both the discontinuity in the moderator material and the strong absorbing canisters had interesting implications for the RAPID code. The axial translation technique utilized by RAPID was not feasible, requiring an axially detailed fission matrix to model this benchmark problem appropriately. The title of the experiment is *Four 4.738 Wt. % Enriched UO_2 Rod Assemblies Contained in Cadmium, Borated Stainless Steel, or Boral Square Canisters, Water-Moderated and Reflected.* Figure 4.7 provides an image of the four canisters out of water, provided by the handbook.

As the title states, it consists of four assemblies, each containing 324 (18x18) fuel rods and surrounded by a varying absorber material. The experiment had 26 cases, as they varied both absorbing canister material and assembly spacing. Case 21 was the selected case for benchmarking in RAPID. It had an assembly spacing of 2 cm, a critical water height of 50.11 cm, and the assemblies were encased in a stainless steel and cadmium absorbing canister. Extensive sensitivity testing was done in the associated review document, as this experiment had a more complicated geometry than the previous two experiments described. The important aspect of this model is that all four of the assemblies are surrounded by a strong absorber (cadmium), lowering k_{eff} by up to 10% in some cases. This has a significant effect on the FM

coefficients.

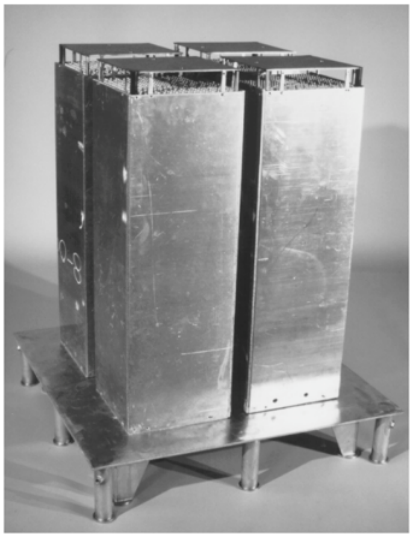

Figure 4.7: Picture of the Fuel Arrays in their Canisters for Benchmark Problem 3 [1]

Benchmark Specifications

The review document goes into detail of two different benchmark models proposed. There is a complete model which can be made, and a simplified version produced from removal of structural materials and simplifications of the fuel arrays and absorbing canisters. Since the simplified version was used for this work, it will be explained in more detail. Sensitivity study results stated that a lot of materials in the fuel rods could be homogenized and structures simplified or removed. Here is the list of the simplifications as described in the review document.

1. The pedestal, 20 cm high, reduced to the Z2 CN18-10 stainless steel support plate 95x95 cm, 0.8 cm thick.

2. The water up to the critical height, under the pedestal support plate (19.2 cm), inside and around the fuel arrays, and around the absorbing canisters to the

edges of the experimental tank.

3. Four fuel assemblies, each including:
    - Four absorber plates replaced by a square section tube (28.8x28.8 cm inside, 29.46 x 29.46 cm outside), 106 cm high for cadmium.
    - The bottom support plate.
    - The lower grid.
    - The fuel rod array up to the critical water level, with a cylindrical shaped bottom plug.
    - The fuel rod array between the critical water level and the top of the fissile column.
    - The two tie rods up to the critical water level.

Structures above the active fuel height were removed, leaving only the fuel rods and absorbing canisters. Finally, the instrumentation thimbles used to house BF_3 counters were removed and replaced with fuel rods, as this proved to have a negligible effect on k_{eff}. From the sensitivity study results and the changes imposed, the benchmark model k_{eff} was determined to be $k_{eff} = 1.00000 \pm 0.00470$ for all cadmium cases with a water gap thickness of 2 cm or greater. Figure 4.7 provides an image of the four canisters out of water, provided by the review document.

4.2.4 Benchmark Problem 4: LEU-COMP-THERM-046

Introduction

This experiment is titled *Critical Loading Configurations of the IPEN/MB-01 Reactor Considering Temperature Variation from 14°C to 85°C*. The IPEN/MB-01 research reactor facility is located in São Paulo, Brazil. This reactor is a "zero power"

(100 watts) reactor used for reactor physics research, and first achieved criticality in 1988. This set of water-moderated square-pitched lattice criticality experiments were conducted in 2008. There are 22 different critical loadings, varying in temperature. The critical loading modeled in this thesis is shown in figure 4.8.

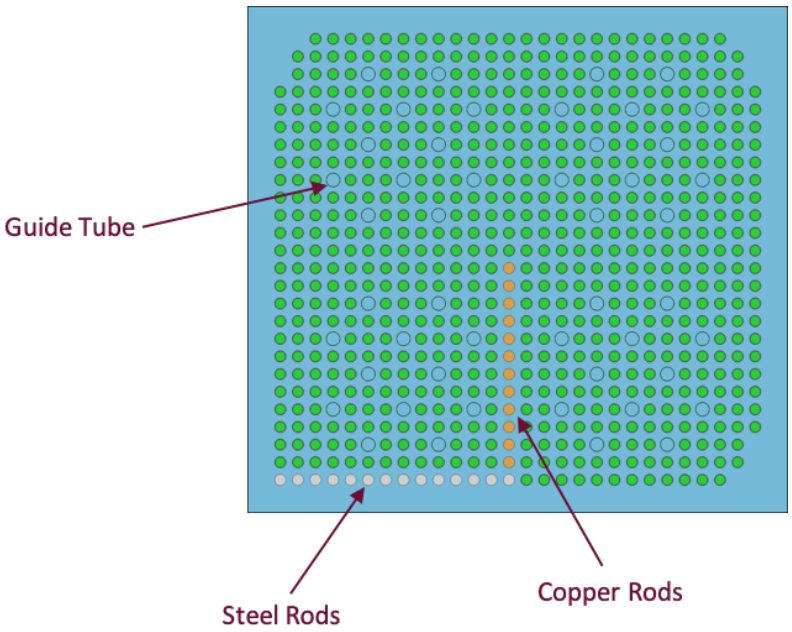

Figure 4.8: Core Loading for Benchmark Problem 4

This is another very small system, and allows for the further exploration of RAPID full fission matrix calculations on a small scale. While benchmark problem 1 had a total of 840 fuel rods, this model contains only 642 fuel rods, alongside copper rods, stainless steel rods, and 48 guide tubes meant to hold control and safety rods. The active fuel height is also quite short, at 54.6 cm. This variation of materials will provide us an analysis of an even smaller system with a non-symmetric fission distribution, which is unique compared to the previous three benchmark problems.

Benchmark Specifications

Case 21 from the hadnbook was modeled because it provided an interesting geometry, and was run at a higher temperature than any of my previous benchmark models. This case was run at 50°C, compared with 20°C (room temperature) in my other benchmarks. The UO_2 fuel rods contained uranium enriched to 4.3486 wt.% ^{235}U. Included in the benchmark models are as follows:

1. The UO_2 fuel rods, encased in type 304 stainless steel cladding, with an outer radius of 0.42447 cm.
2. The copper rods, with an outer radius of 0.475 cm.
3. The type 304 stainless steel rods, with an outer radius of 0.475 cm.
4. The guide tubes for safety and control rods, filled with water, with an outer radius of 0.600 cm.
5. The bottom of the withdrawn Ag-In-Cd control rods near the top of the geometry.
6. A 2.2 cm thick, 58.8 cm square of type 304 stainless steel serving as the lower grid plate.
7. A cylinder of water starting 30 cm below the grid plate and ending at the top of the fuel, with a radius of 91.5 cm.

Figure 4.9 is obtained from the reference document, and shows a detailed cross-sectional diagram of the different rods in the core loading (although this case did not use the $UO_2Gd_2O_3$ rods shown). The benchmark specification for this case is $k_{eff} = 1.00039 \pm 0.00044$.

The following chapters give the computational model for each benchmark problem, and present results and their implications. For each benchmark problem, a Serpent

reference calculation is performed to compare with the RAPID calculated eigenvalue and fission density. The first two benchmark problems discussed also include comparisons of results calculated using RAPID's axial translation approach.

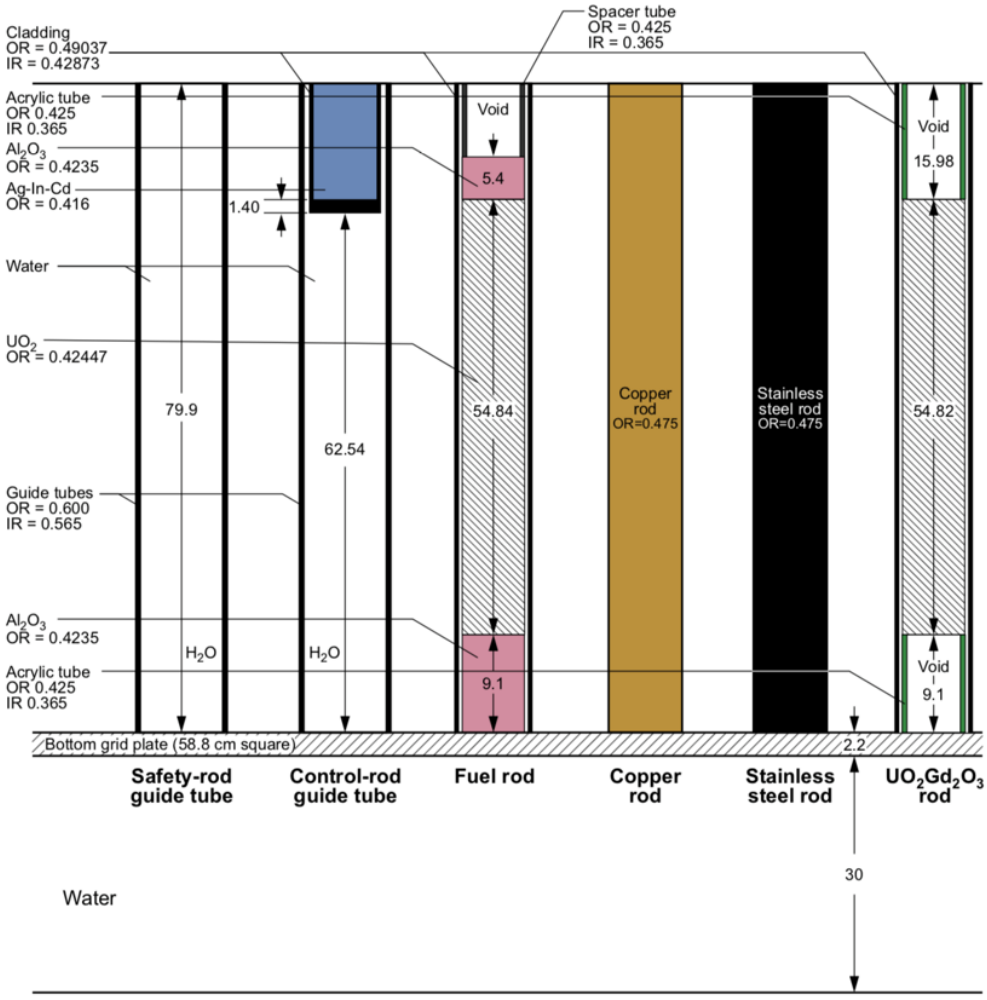

Figure 4.9: Axial Schematic of Different Rods for Benchmark Problem 4 [1]

Chapter 5

Source Convergence Study

In an eigenvalue Monte Carlo calculation, three parameters including number of particles per cycle, number of inactive (skipped) cycles, and number of active cycles need to be chosen appropriately in order to achieve precise and unbiased solutions. To determine an appropriate set of parameters to use for this thesis, a source convergence study was performed, using benchmark problem 1. This stemmed from the fact that the provided sample calculations given in the ICSBEP review document often were fairly quick calculations, with particularly large uncertainties on k_{eff}. For example, the sample calculation provided for case 7 was run with MCNP, using a continuous-energy ENDF/B-V cross section library. Their choice of parameters was 1500 particles per generation, with 50 skipped cycles and 110 active cycles. They obtained a k_{eff} of 0.99680, with a 1σ uncertainty of 0.00170, far too different to be used as a benchmark reference model. The performed convergence study involved 35 separate runs of this model using Serpent with the continuous-energy ENDF/B-VII cross section library. The goal was to find an ideal set of parameters that gave good statistics with a manageable computational requirement.

The parameters for the source convergence study varied as follows. The number of

particles per generation ranged from 1,500 to 500,000, as 1,500 particles per cycle was used in the provided sample calculation. 500,000 particles per cycle was arbitrarily chosen, leaving room to increase the parameter if necessary, although results show it wasn't necessary to go beyond 500,000 particles for a well converged result. The number of active cycles tested for all particle numbers ranged from 100 to 250, and the number of skipped cycles ranged from 50 to 250. It was quickly understood that a minimum of 50 skipped cycles was needed, as anything less gives an unconverged fission source, shown in run 1. The data collected from each run was the calculated implicit k_{eff}, its associated uncertainty, and the weighted uncertainty on the fission density. The results of the source convergence study led to the conclusion that a minimum of 500,000 particles per cycle, 250 active cycles, and 50 inactive cycles were needed to obtain a converged result in both eigenvalue and fission density. This combination of parameters kept the uncertainty on k_{eff} to less than 10 per cent milli (pcm) and the weighted average uncertainty on fission density tallies to less than 1%.

The weighted relative uncertainty for fission density is calculated by:

$$Wgtd.\ Rel.\ Uncertainty = \frac{\sum_{j=1}^{N} x_j * \sigma_j}{\sum_{j=1}^{N} x_j} \tag{5.1}$$

Where x_j is the fission density at location j and σ_j is the uncertainty on the fission density x_j.

This approach of examination of both eigenvalue and fission density is essential to achieve confidence in the selected combination of run parameters.

Run	NPS	Particles/Region	Active	Skipped	k_{eff}	Uncertainty, 1σ	Wgtd. Uncertainty on Fission Density
1	1500	0.049	110	10	0.99881	0.00183	0.42629
2	1500	0.049	110	50	0.99967	0.00198	0.26862
3	1500	0.049	500	250	0.99638	0.00098	0.13154
4	10000	0.33	100	50	0.99704	0.00084	0.11290
5	10000	0.33	150	50	0.99812	0.00068	0.07997
6	10000	0.33	200	50	0.99791	0.00058	0.09228
7	10000	0.33	250	50	0.99832	0.00052	0.07157
8	50000	1.65	100	50	0.99877	0.00036	0.05062
9	50000	1.65	150	50	0.99793	0.00030	0.04134
10	50000	1.65	200	50	0.99791	0.00026	0.03584
11	50000	1.65	250	50	0.99844	0.00023	0.03205
12	100000	3.30	100	50	0.99848	0.00026	0.03585
13	100000	3.30	150	50	0.99823	0.00021	0.02924
14	100000	3.30	200	50	0.99825	0.00018	0.02533
15	100000	3.30	250	50	0.99842	0.00016	0.02264
16	200000	6.60	100	50	0.99767	0.00018	0.02534
17	200000	6.60	150	50	0.99799	0.00015	0.02070
18	200000	6.60	200	50	0.99819	0.00013	0.01792
19	200000	6.60	250	50	0.99804	0.00012	0.01603
20	300000	9.90	100	50	0.99807	0.00015	0.02067
21	300000	9.90	150	50	0.99813	0.00012	0.01689
22	300000	9.90	200	50	0.99806	0.00010	0.01462
23	300000	9.90	250	50	0.99803	0.00009	0.01308
24	400000	13.20	100	50	0.99829	0.00013	0.01790
25	400000	13.20	150	50	0.99824	0.00011	0.01462
26	400000	13.20	200	50	0.99807	0.00009	0.01266
27	400000	13.20	250	50	0.99828	0.00008	0.01133
28	500000	16.50	100	50	0.99842	0.00012	0.01601
29	500000	16.50	150	50	0.99811	0.00009	0.01307
30	500000	16.50	200	50	0.99825	0.00008	0.01133
31	500000	16.50	250	10	0.99797	0.00007	0.01014
32	500000	16.50	250	50	0.99820	0.00007	0.01013
33	500000	16.50	250	100	0.99819	0.00007	0.01013
34	500000	16.50	250	150	0.99818	0.00007	0.01013
35	500000	16.50	250	200	0.99817	0.00007	0.01013

Table 5.1: Convergence Study Data

5.1 Analysis of Skipped Cycle Parameter

Observing runs 31 to 35 in table 5.1, all have less than a 10 pcm uncertainty on k_{eff} and a 1% mean weighted uncertainty on the fission density. However, further detail is needed to observe how the source distribution changes with the variation of the skipped cycles parameter. It is logical to assume the most converged calculation would be run 35, as it has the largest number of particles in combination with largest number of skipped cycles. Using this run as the reference point for a converged fission source, the point at which increasing the number of skipped cycles stops changing the resulting fission source can be determined, establishing a value that allows for proper convergence.

This can be shown through taking the average relative differences in fission densities between runs 31 to 34 and run 35. Table 5.2 shows the data for this test. Values calculated are the mean relative differences in fission density, and the standard deviation on the mean relative difference.

Run	NPS	Active	Skipped	Rel. Diff. (%)
31	500,000	250	10	0.36
32	500,000	250	50	0.17
33	500,000	250	100	0.17
33	500,000	250	150	0.15

Table 5.2: Mean Relative Differences, Varying Skipped Cycles

From this table, the runs using 50, 100, and 150 skipped cycles all have similar relative differences in fission source compared to the more accurate run with 200 skipped cycles. This indicates that they are converged, with the run with 10 skipped cycles is significantly different. This justifies using a minimum of 50 skipped cycles for the Serpent reference calculations performed in this thesis.

Figure 5.1 further illustrates that the 10 skipped cycles is not sufficient, leading to an inaccurate estimate of k_{eff}.

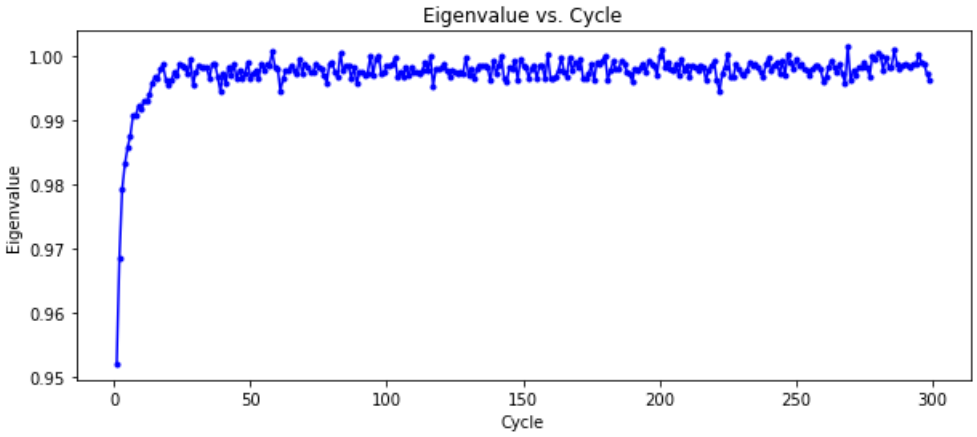

Figure 5.1: Eigenvalue vs. Cycle

Figure 5.2 shows how the uncertainty on k_{eff} drops as the number of active cycles increases. These figures show data obtained from run 32 in the convergence study.

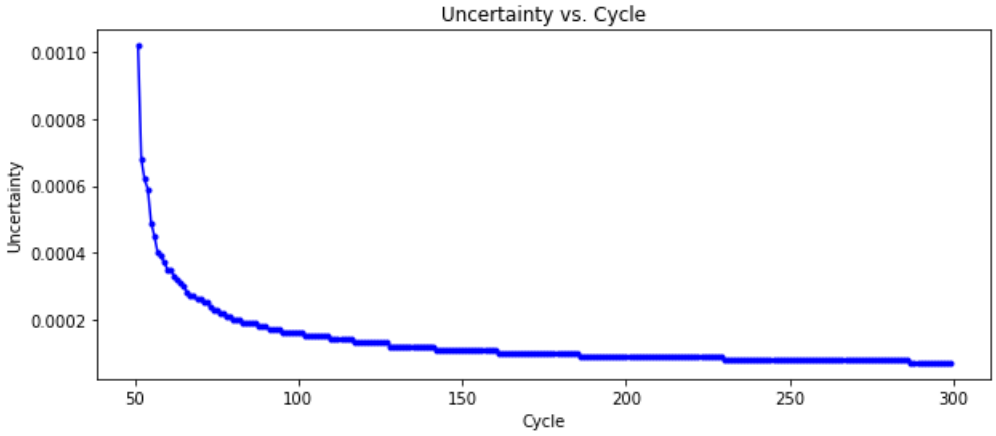

Figure 5.2: Uncertainty vs. Cycle

5.2 Analysis of Active Cycle Parameter

Given that the number of skipped cycles that has been selected appropriately, increasing the number of active cycles decreases the uncertainty on both k_{eff} and on the source distribution. If the number of particles per cycle and number of skipped cycles are held constant, the number of active cycles can be varied to show the decrease in uncertainties on both k_{eff} and the weighted relative uncertainty on the fission density. In table 5.3, the number of active cycles is varied while the number of particles per cycle is held to 500,000 and the number of skipped cycles is held to 50. Referring back to table 5.1, observe that this decrease in uncertainty is shown for all variations of NPS.

NPS	Active	Skipped	Uncertainty on k_{eff}	Wgtd. Unc. on Fission Density
500000	100	50	0.00012	0.01601
500000	150	50	0.00009	0.01307
500000	200	50	0.00008	0.01133
500000	250	50	0.00007	0.01013

Table 5.3: Variation of the Number of Active Cycles

As this is one of the two parameters that simply improve the statistics of the model, 250 active cycles is recommended for use in the Serpent reference calculations.

5.3 Analysis of NPS Parameter

Similar to the variation of the active cycles, it is easy to observe a decrease in the uncertainty estimates on k_{eff} and the fission source through the increase of the number of particles per cycle. In table 5.4, the number of active cycles is held to 250, the number of skipped cycles is held to 50, and the number of particles per

cycle is varied. Also shown is the number of particles per tally region, which gives a parameter which is applicable to all four of the Serpent reference calculations.

NPS	Particles/Region	Active	Skipped	Uncertainty on k_{eff}	Wgtd. Unc. on Fission Density
10000	0.33	250	50	0.00052	0.07157
50000	1.65	250	50	0.00023	0.03205
100000	3.30	250	50	0.00016	0.02264
200000	6.60	250	50	0.00012	0.01603
300000	9.90	250	50	0.00009	0.01308
400000	13.20	250	50	0.00008	0.01133
500000	16.50	250	50	0.00007	0.01013

Table 5.4: Variation of the NPS Parameter

At this point, it is suggested that each Serpent reference calculation uses an NPS selection that provides at least 16.5 particles per tally region. For this reason, each of the Serpent reference calculations used an NPS value 10^6 to accommodate the larger benchmark problems modeled.

Chapter 6

Benchmark Problem 1

6.1 Serpent Reference Calculation

6.1.1 Model Description

As stated in the introduction to selected benchmarks, case 7 from the experiment was used for benchmarking. It consisted of three fuel rod clusters in a line, each containing $20 * 14 = 280$ UO_2 fuel rods, enriched to 2.35 wt.% ^{235}U. These clusters were placed on top of an acrylic support/reflector plate, in a pool of light water at room temperature. The benchmark model removes all materials except for the fuel rods, the water, and the lower reflector plate. The benchmark specified criticality eigenvalue is $k_{eff} = 0.99980 \pm 0.00310$. The benchmark geometry generated by Serpent is shown in figure 6.1 and 6.2, with relevant dimensions included.

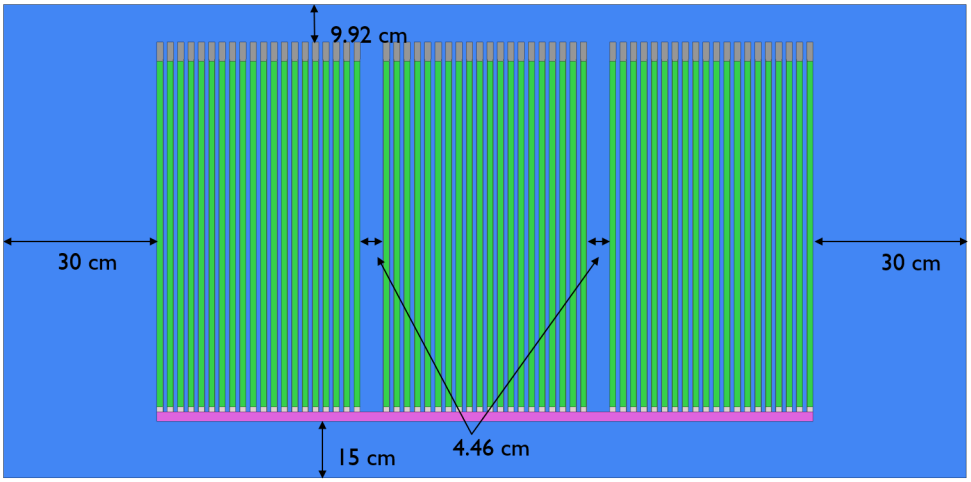

Figure 6.1: X-Z View of Benchmark Problem 1

6.1.2 Serpent Reference Calculation Results

The Serpent reference calculation was performed with 10^7 particles per cycle, with 500 active cycles and 250 skipped cycles. The goal was to get the highest resolution on fission density as realistically obtainable, and to get a close k_{eff} result to the benchmark value. Serpent calculations yielded a $k_{eff} = 0.99821 \pm 0.00001$, with a weighted fission density uncertainty of 0.26%, far below my goal threshold of 10pcm uncertainty on k_{eff} and 1% on weighted fission density uncertainty. This determined k_{eff} is -159pcm below the benchmark $k_{eff} = 0.99980$.

The fission density and associated uncertainty are shown in figures 6.3a and 6.3b, respectively. The plots were sliced down the middle to show the inside behavior of the model, particularly the regions of high fission density right outside the central assembly. This is due to the small assembly spacing of the model, resulting in a peak in the fission densities of the side assemblies.

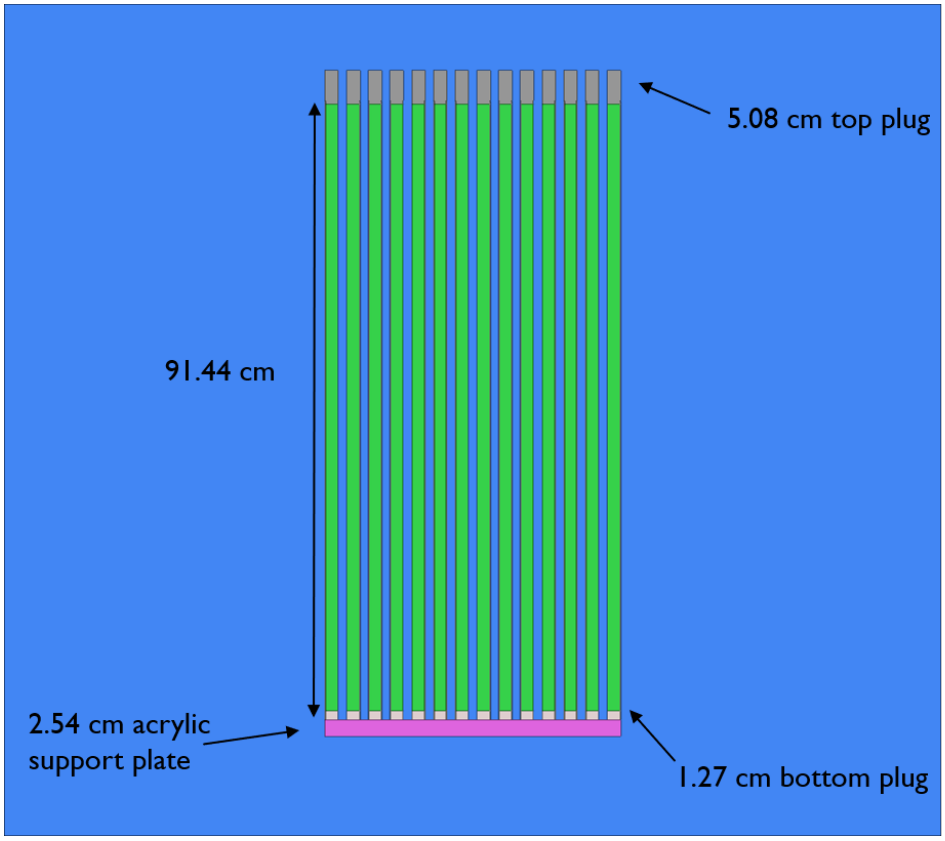

Figure 6.2: Y-Z View of Benchmark Problem 1

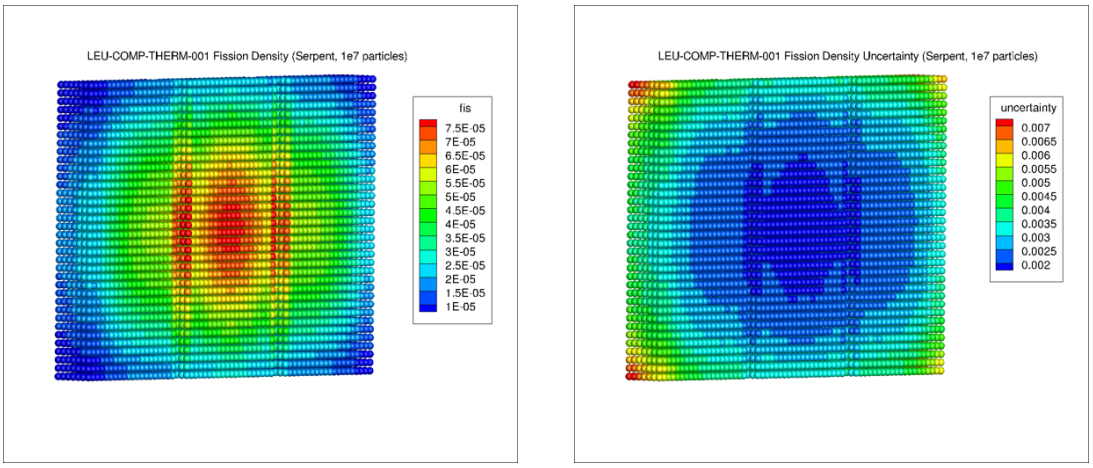

(a) Fission Density (b) Uncertainty

Figure 6.3: Serpent Fission Density and Uncertainty for Benchmark Problem 1

6.2 RAPID Results

6.2.1 Standard pRAPID

After an appropriate Serpent reference calculation was performed, the geometry is then used as the basis for FM coefficient calculations in pRAPID. FM coefficient calculations consist of a set of fixed-source calculations, placed in each axial location of each fuel rod. Using this methodology, a total of 280 pre-calculations are necessary, with one calculation being performed at the central axial level in each fuel rod of the central assembly. When processed, it forms the full fission matrix, although simplifications can lead to a significant reduction in the amount of coefficient calculations needing to be performed. By default, pRAPID generates coefficient calculation files for a central cluster, at the central axial level. Coefficient data is then mapped to other clusters assumed to have the same behavior and then translated axially up the top half of the model. It is then finally projected across the z-axis to get a complete fission matrix. These techniques reduce pre-calculation requirements substantially. The axial translation and cluster mapping techniques weren't accurate in the cases of

the small benchmark problems examined in this thesis, although it served as a good starting point and justified the need for more detailed calculations. Shown below are log plots of coefficients with the source located at three different positions in the central cluster. The coupling of fission between fuel clusters is more evident when observing the coefficient plots on the edge and corner of the cluster.

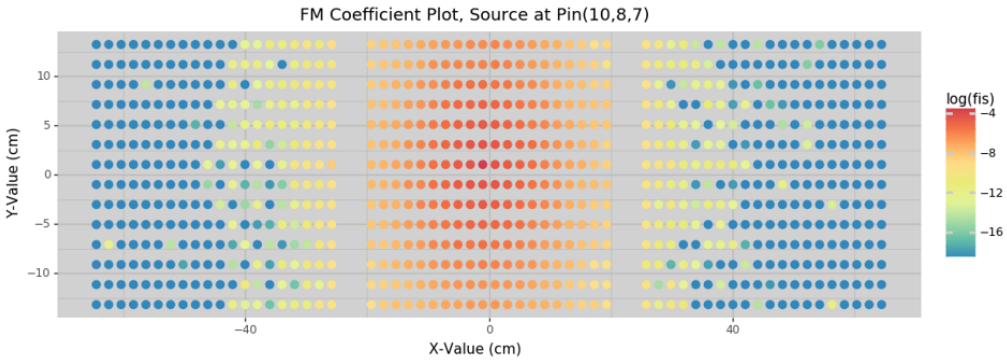

Figure 6.4: FM Coefficient Plot, Source at X=10, Y=8, Z=7, Benchmark Problem 1

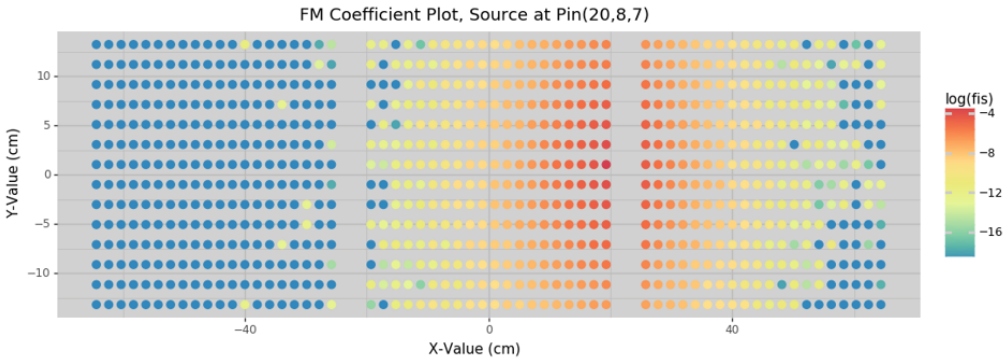

Figure 6.5: FM Coefficient Plot, Source at X=20, Y=8, Z=7, Benchmark Problem 1

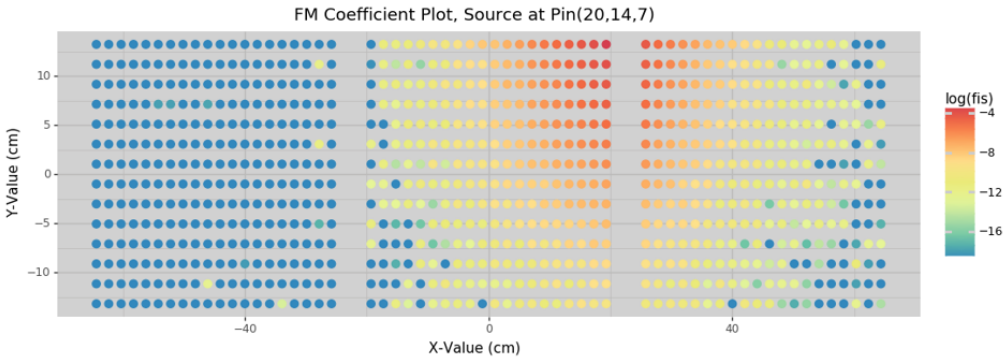

Figure 6.6: FM Coefficient Plot, Source at X=20, Y=14, Z=7, Benchmark Problem 1

Each FM coefficient calculation was run with 10^6, 10^7, and 10^8 particles. Multiple sets of coefficients with varying numbers of particles were used to examine the uncertainty as particles increased, and to compare with calculation time and ultimately, the k_{eff} result. The uncertainty plots shown in figure 6.7 show expected behavior from an increased amount of particles, they reach further out in the model and the uncertainty subsequently drops. The data in table 6.1 shows the increase in total pre-calculation time with increasing NPS, largely matching the exponential increase in particles run. Also shown is the number of particles per tally region. It is clear that the 10^8 case has an excessive number of particles.

NPS	Particles/Region	Time/1 Coefficient (min.)	Time/All Coefficients (min.)
10^6	33.06	1.6	448
10^7	330.6	12.2	3416
10^8	3306	124.1	34748

Table 6.1: Time for FM Coefficient Calculation, Varying Number of Particles

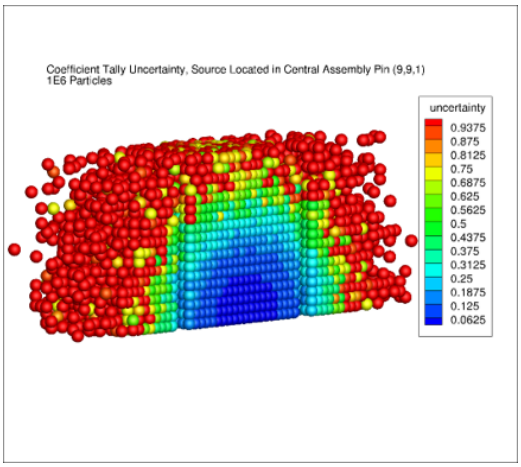

(a) 10^6 Particles

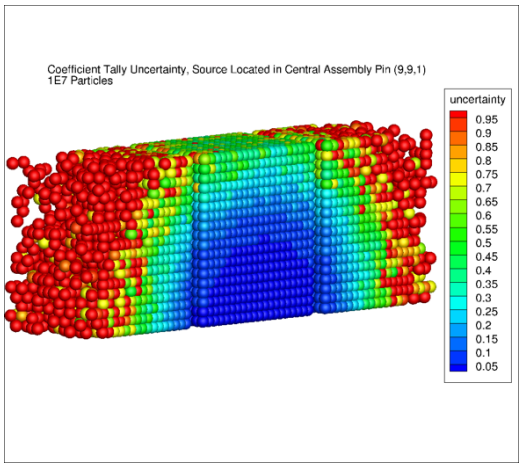

(b) 10^7 Particles

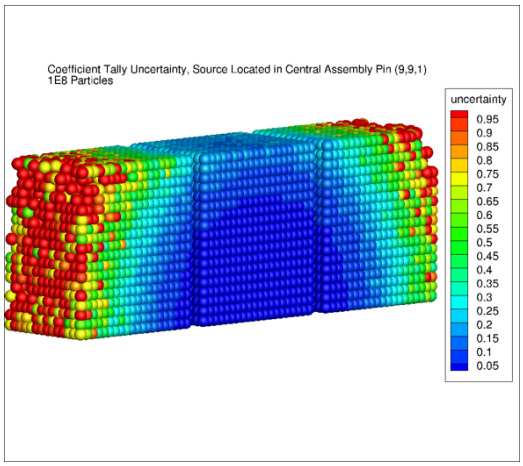

(c) 10^8 Particles

Figure 6.7: FM Coefficient Uncertainty for Benchmark Problem 1, Varying Particles

Table 6.2 compares the RAPID calculated k_{eff} (for differing NPS) to that of the experimental result and the Serpent reference calculation. The results show no significant difference in the eigenvalue calculation when varying the number of particles, varying by no more than 10 pcm. This suggests that all three numbers are sufficient. These results as they stand are not satisfactory and further studies are necessary.

Model (NPS)	Particles/Region	k_{eff}	Rel. Diff. (pcm)	Time (min.)	# Cores
Experiment	–	0.99980 ± 0.00310	–	–	–
Serpent (10^7)	330.6	0.99821 ± 0.00002	-159	491	8
RAPID (10^6)	33.06	0.99490	-490	4	1
RAPID (10^7)	330.6	0.99500	-480	4	1
RAPID (10^8)	3306	0.99497	-483	4	1

Table 6.2: Standard RAPID Results for Benchmark Problem 1

Three further coefficient generation schemes are examined including:

1. Boundary correction to the standard set of FM coefficients
2. Generation of FM coefficients the central axial level of each fuel rod
3. Full fission matrix calculation containing detailed axial information

Boundary Correction

In this study, since the central cluster is only surrounded by clusters on two sides, and surrounded by water on the other two, that behavior needed to be examined on the outer clusters too. To achieve this, the correction model consisted of five clusters in a line, instead of the three described in the benchmark model.

The boundary correction ratio defined in equation 3.1 is applied to the uncorrected FM coefficients as expressed by equation 3.2. This leads to the boundary correction ratio plot which is provided in figure 6.8. The increased fission towards the edge is

due to moderation effects in the reference model that aren't present in the correction model. Applying this ratio to the fission matrix allows for the modeling of a fission distribution more similar to the exact distribution, and in this case would bring k_{eff} up towards the experimental value.

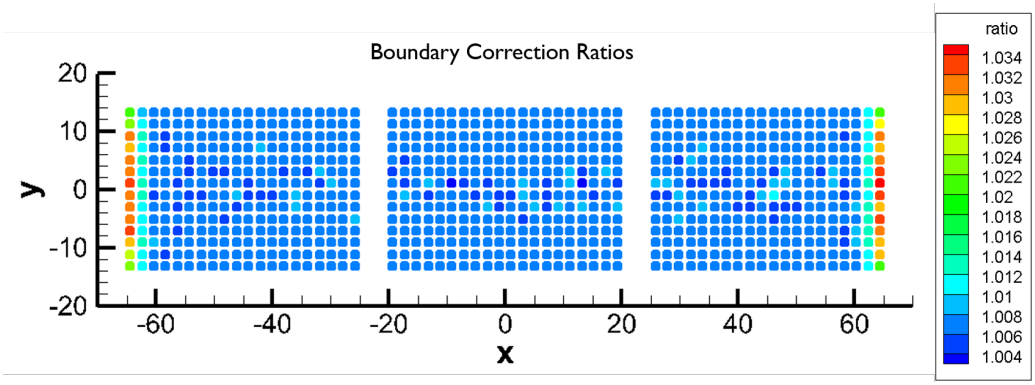

Figure 6.8: Boundary Correction Ratio Plot for Benchmark Problem 1

The boundary correction file was applied to the 10^8 set of coefficients previously used. The results show that the k_{eff} increased by about 700 pcm, a very drastic swing upwards, from $k_{eff} = 0.99497$ to $k_{eff} = 1.00192$. While this result is now well within the 1σ uncertainty on k_{eff}, the feasability of this method for similar problems needs to be studied.

6.2.2 Improved Models

Radially Detailed FM Coefficient Model

In order to examine the boundary correction method is an overcorrection, FM coefficients in each fuel pin across the three assembly model were calculated, thus eliminating the need for any boundary correction. To adapt this capability into RAPID and pRAPID, the *xy-mode* flags had to be added, as described in section A.

Example plots of the coefficient calculation and associated uncertainty from this

coefficient scheme are shown in figures 6.9 and 6.10, respectively. Notice that this is still a top half coefficient model, so this plot is reflected down to obtain a full fission matrix. This option has been well integrated into both pRAPID and RAPID for further use in other applications, however, proved to not be applicable to this model given the failure of the axial translation scheme. Table 6.3 shows the updated RAPID results for this model. It results for the radially detailed FM coefficients, followed by the standard set of coefficients with and without boundary correction.

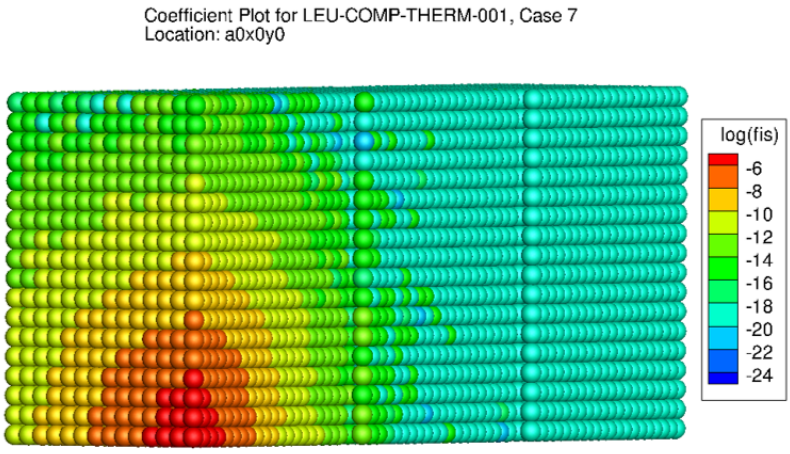

Figure 6.9: FM Coefficient Plot in Radially Detailed Model, Benchmark Problem 1

Model	k_{eff}	Rel. Diff. (pcm)	Time (min.)	# Cores
Experiment	0.99980 ± 0.00310	–	–	–
Serpent	0.99821 ± 0.00002	-159	491	8
RAPID	0.99500	-480	3.73	1
RAPID w/ Boundary Corr.	1.00195	+215	5.88	1
RAPID w/ Radially Detailed Coeffs	0.99519	-461	1.5	1

Table 6.3: Results Comparison for Benchmark Problem 1

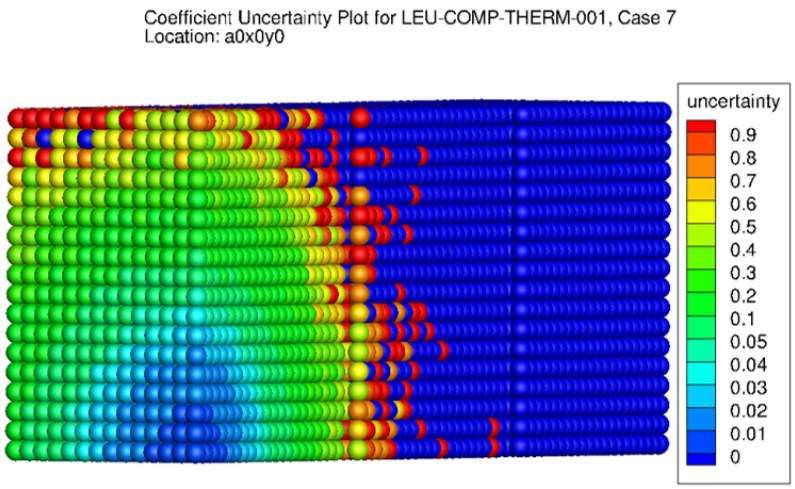

Figure 6.10: FM Coefficient Plot Uncertainty in Radially Detailed Model, Benchmark Problem 1

Full Fission Matrix

As it has been laid out, all of the previous coefficient generation schemes fall short of the target accuracy of within the 1σ uncertainty put forth by the benchmark specifications. If the techniques RAPID uses to minimize the number of FM coefficients needed to fill the fission matrix are ignored, and instead using a brute force approach, a very detailed and accurate calculation can be performed, obtaining a result that ideally falls within the benchmark uncertainty. This requires generating a lot more FM coefficients, which takes considerable computing power. In this model, a total of 30,240 FM coefficients is required for a full fission matrix calculation. As this would be particularly cumbersome in calculation time all around, the existing quarter symmetry was considered. This resulted in a redutction of the number of pre-calculations by 75%, down to 7,560.

Although it was expected that the use of the physical symmetry would yield an accurate fission density distribution, a full reference was created to determine the "exact" fission density distribution. Figure 6.11 compares the fission densities calcu-

lated with the two models. The average relative difference between the two models is 0.0028%, indicating that the two distributions are identical.

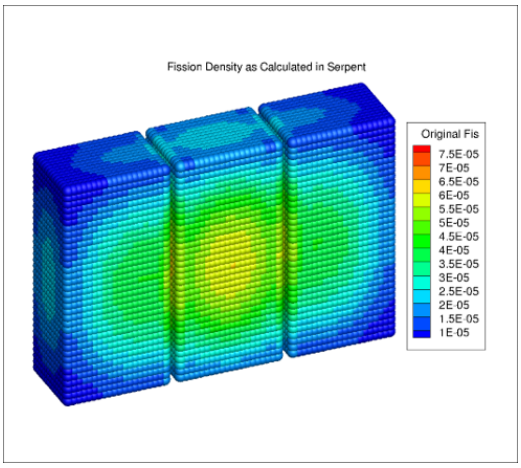

(a) Original Serpent FD

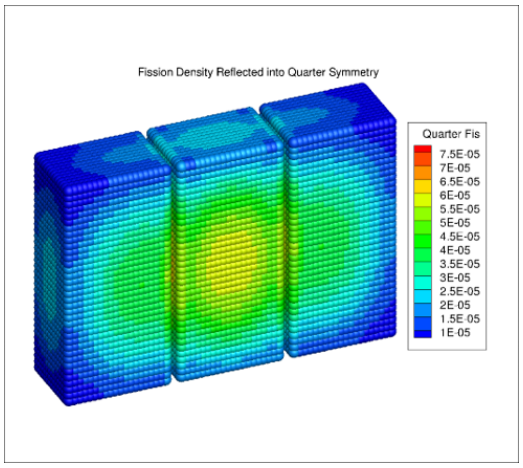

(b) Serpent FD, $\frac{1}{4}$ Symmetry

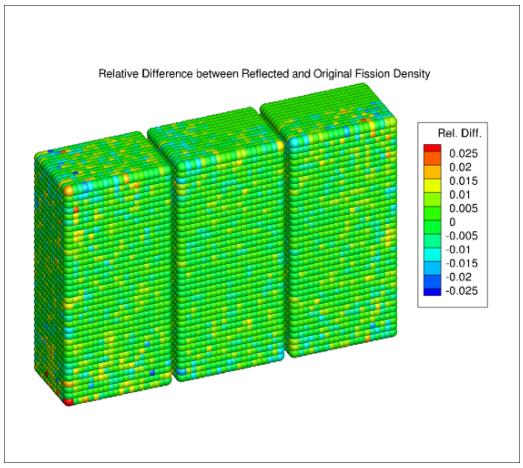

(c) Relative Difference (Absolute)

Figure 6.11: Original vs. $\frac{1}{4}$ Symmetry Fission Density

RAPID Full FM Results

Overall, these results gave the most detail of all of the RAPID models created for this benchmark problem. Table 6.4 compares the k_{eff} obtained by RAPID with the Serpent prediction and the experimental data.

Model	k_{eff}	Rel. Diff. (pcm)	Time (min.)	# Cores
Experiment	0.99980 ± 0.00310	–	–	–
Serpent	0.99821 ± 0.00005	-159	491	8
RAPID (Full FM)	0.99752	-228	114	1

Table 6.4: Model Results Summary for Benchmark Problem 1

The above table indicates that the RAPID results yields a solutions within the experimental results. Furthermore, figure 6.12 shows that RAPID's fission density distribution is in excellent agreement with the Serpent results, while still providing a speedup of 4x using only 1 core, as opposed to 8 cores in the Serpent calculation.

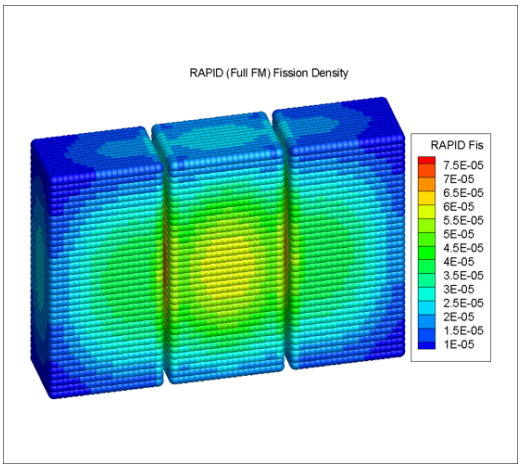

(a) RAPID FD

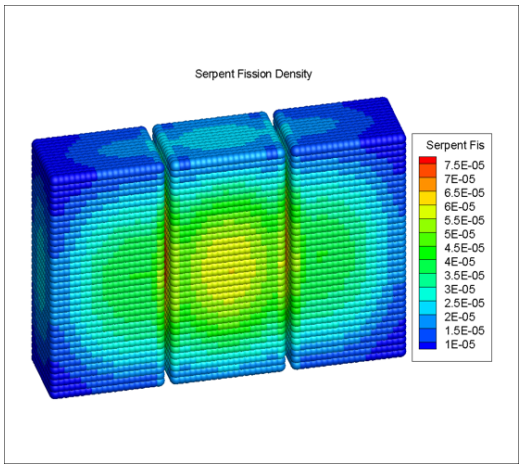

(b) Serpent FD

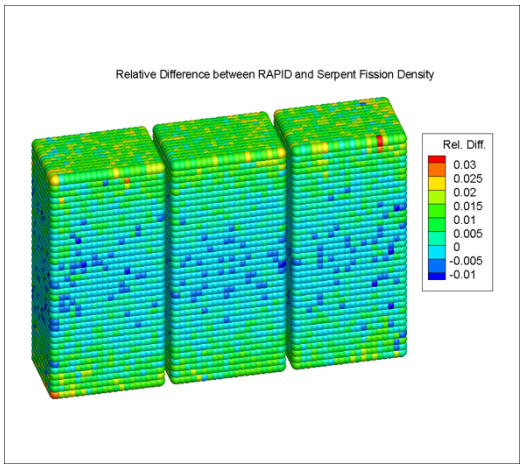

(c) Relative Difference (Absolute)

Figure 6.12: RAPID vs. Serpent Fission Density for Benchmark Problem 1

Chapter 7

Benchmark Problem 2

7.1 Serpent Reference Calculation

7.1.1 Model Description

This experiment was another critical approach experiment consisting of rectangular clusters of UO_2 fuel rods. The key changes compared to the previous benchmark problem studied were the increase in ^{235}U enrichment from 2.35% to 4.31%, the presence of steel reflecting walls along the line of fuel clusters, and the presence of absorber plates between the clusters, up against the central cluster. The rod pitch was now 1.892 cm instead of 2.032 cm. Case 1 was studied in detail, with the absorber plate material being type 304-L stainless steel, with a thickness of 0.302 cm, and a critical cluster separation of 13.273 cm. Each cluster contained 192 (12x16) rods, and the model was run using one axial level per inch of fuel, or in this case 36 axial levels. The geometry defined by Serpent is shown in figure 7.1.

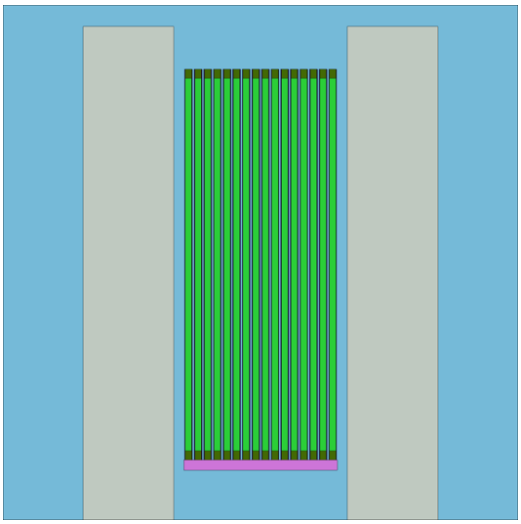

(a) YZ View

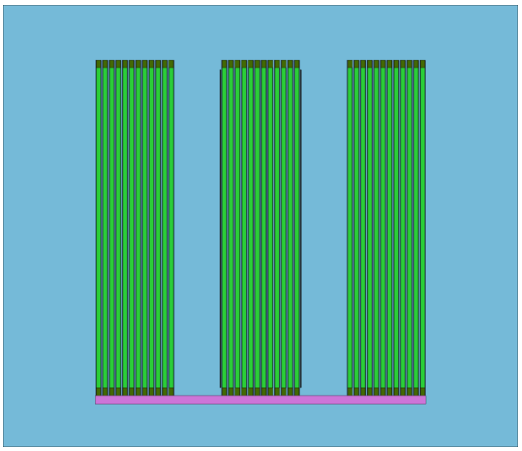

(b) XZ View

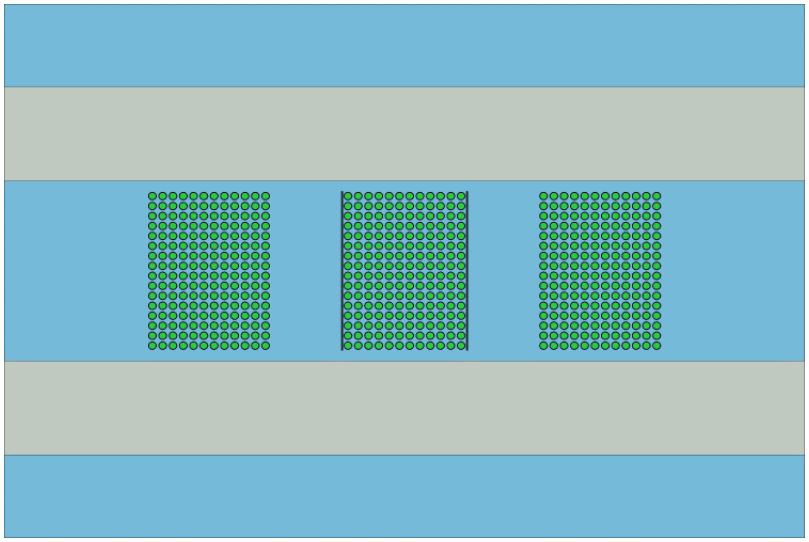

(c) XY View

Figure 7.1: Serpent Geometry for Benchmark Problem 2

7.1.2 Serpent Reference Calculation Results

The reference model created in Serpent was run with 10^6 particles, 250 active cycles, and 100 skipped cycles. This led to a weighted fission density uncertainty of 0.91%, under the weighted fission density uncertainty threshold suggested in my source convergence study. Table 7.1 shows the Serpent results compared to the experimental value.

Model	Particles/Region	k_{eff}	Rel. Diff. (pcm)	Time (min.)	# Cores
Experiment	–	1.00000 ± 0.00180	–	–	–
Serpent	48.22	1.00182 ± 0.00006	+182	252	8

Table 7.1: Serpent Reference Calculation Results for Benchmark Problem 2

The above results indicate that the Serpent uncertainty is 180 pcm below the benchmark k_{eff}. The fission density and associated uncertainty for this model are shown in figure 7.2. The highest uncertainty is in the outer corners of the model, with a peak at around 1.8% uncertainty. The interesting thing here is the noticeable reduction in fission density on the outside of the central assembly, as the steel absorber plates are doing their job. Without them, the fission density would be much higher, similar in behavior to the inside of the outer assemblies.

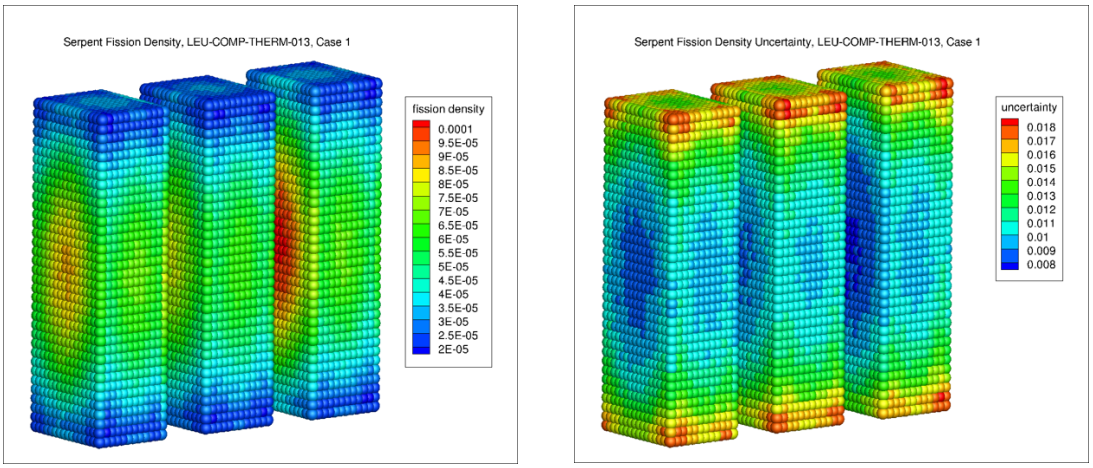

(a) Fission Density (b) Uncertainty

Figure 7.2: Serpent Fission Density and Uncertainty for Benchmark Problem 2

7.2 MCNP Reference Calculation

The reference document for this model included a sample calculation using MCNP, with the input file. Their choice of parameters in terms of cycles and number of particles per cycle seemed like an arbitrary selection. To test whether the sample calculation's run parameters (2500 particles, 60 skipped cycles and 600 active cycles) would lead to an inaccurate eigenvalue estimate, this model was run to compare with the Serpent reference calculation, as well as an MCNP reference calculation using 10^6 particles per cycle, 250 active cycles, and 100 inactive cycles.

Results from both of these MCNP reference calculations are shown alongside the Serpent reference calculation and the experimental value in table 7.2. While the uncertainty on k_{eff} dropped in the refined MCNP reference calculation, the estimate of k_{eff} itself did not change significantly. However, both MCNP calculations underestimated k_{eff} by a significant margin.

Model	$k_{eff} \pm 1\sigma$	Rel. Diff. (pcm)	Time (min.)	# Cores
Experiment	1.00000 ± 00.00180	–	–	–
Serpent (10^6, 250, 100)	1.00182 ± 0.00005	+182	252	8
MCNP (1500, 600, 60)	0.99704 ± 0.00063	-296	2.5	8
MCNP (10^6, 250, 100)	0.99723 ± 0.00006	-277	195	8

Table 7.2: MCNP Eigenvalue Results for Benchmark Problem 2

7.3 RAPID Results

For this benchmark problem, modeling with RAPID included only a radially detailed coefficient model, and a full fission matrix calculation. The former is used to show that FM coefficients calculated using the axial translation method used by RAPID gives an unsatisfactory result for this geometry, and provides justification for the latter model created.

7.3.1 Improved Models

Radially Detailed FM Coefficient Model

Since it was established in the analysis performed in section 6.2.1 that the axial translation method used by RAPID for filling in the fission matrix leads to an inaccurate estimate on k_{eff}, the standard FM coefficient generation method and boundary correction techniques are ignored for this benchmark problem. The only model created in RAPID using the axial translation method is a radially detailed FM coefficient model. This model only required 576 FM coefficients, and the full fission matrix required 20,736 coefficients. In figure 7.3, it is shown that due to the absorber plates and the increased cluster separation, there is not as much coupling in terms of fission density as shown in figure 6.6.

The RAPID calculated eigenvalue using the radially detailed FM coefficient model

gave a result of $k_{eff} = 0.99701$. This is outside the 1σ uncertainty by 120 pcm, but this result was expected given that this small geometry is too small to provide an accurate result using axial translation. Three sets of coefficients were generated by varying the number of particles per FM coefficient calculation. The values tested were 10^5, 10^6, and 10^7. The results in terms of k_{eff} did not change in any significant way.

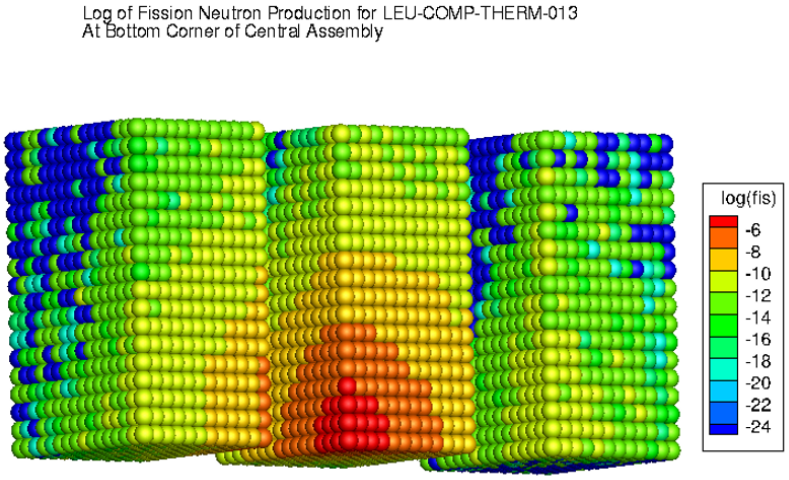

Figure 7.3: FM Coefficient Plot for Benchmark Problem 2

Full Fission Matrix

This was one of two models where all FM coefficients were calculated to fill the full fission matrix. Other models had easily adaptable quarter symmetry which could be used. For this benchmark problem, a full FM calculation was performed in order to study the results of a later axial collapsing study. After the results of this full fission matrix calculation are discussed, axial collapsing testing is performed to measure how RAPID compares to a similarly collapsed Serpent model in terms of both eigenvalue and fission density. FM coefficient calculations required 36 axial levels, with 576 total rods, for a grand total of 20,736 FM coefficients. Figure 7.4 shows an FM coefficient

plot with the source located on the outer side of the left most assembly.

The eigenvalue determined from this calculation was $k_{eff} = 1.00151$, which is only 151 pcm above the experimental value, and within the experimental uncertainty. This result is comparable to the Serpent reference calculation.

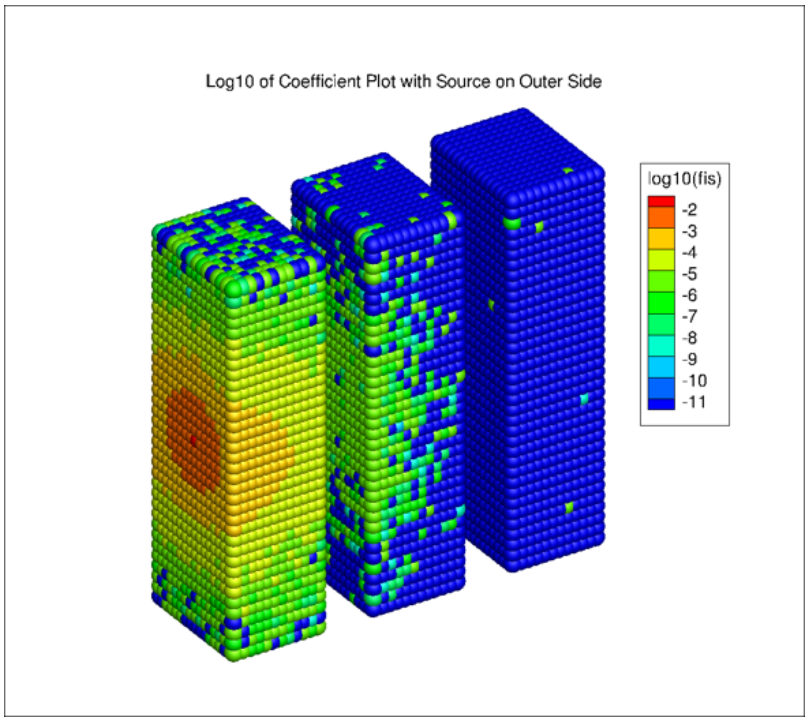

Figure 7.4: Full FM Coefficient Plot for Benchmark Problem 2

Fission density behavior closely matched that of Serpent, with the mean relative difference of 0.17% with the standard deviation on relative difference being 1.21% (see figure 7.5c). This is just saying that almost all of the differences oscillate around zero and can largely be attributed to noise. The only areas of large relative difference were around the top and bottom of the model, which suffer from poor convergence. The fission densities for the full FM RAPID model, the reference Serpent model, and the relative differences are shown in figure 7.5.

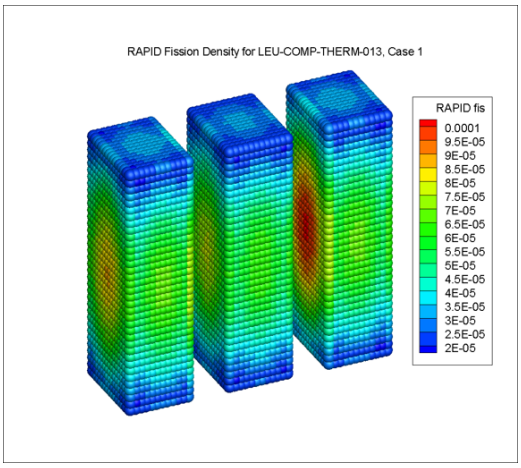

(a) RAPID Full FM

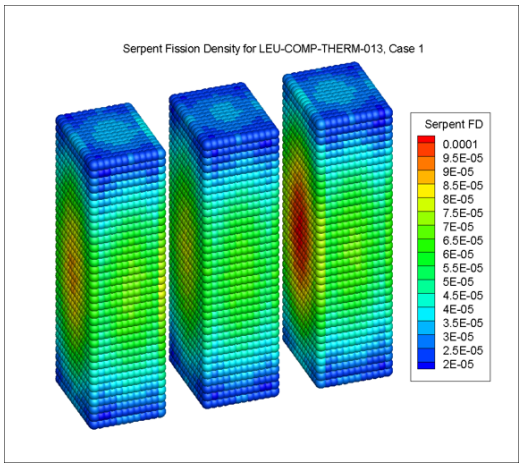

(b) Serpent Reference

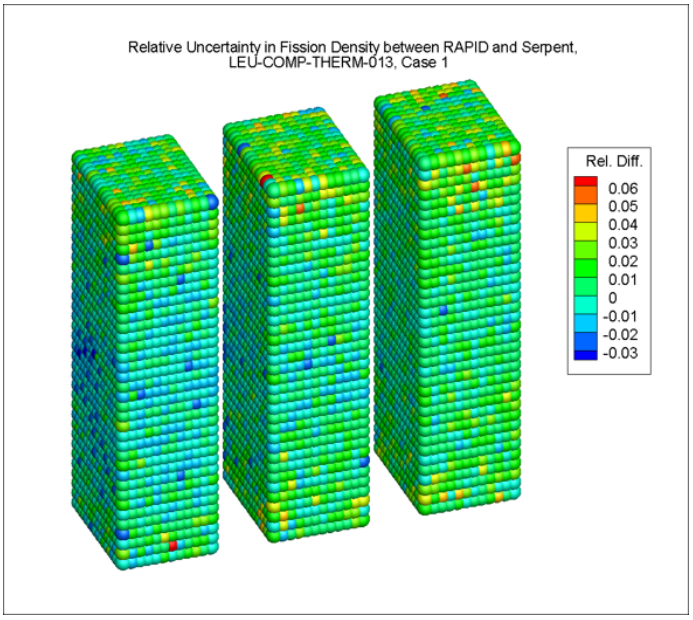

(c) Relative Difference

Figure 7.5: Fission Density Comparison b/t Serpent and RAPID, Benchmark Problem 2

For comparison of all methods explored, the k_{eff} results are presented in table 7.3.

Model	$k_{eff} \pm 1\sigma$	Rel. Diff. (pcm)	Time (min.)	# Cores
Experiment	1.00000 ± 0.00180	–	–	–
Serpent Reference	1.00182 ± 0.00005	+182	252	8
MCNP Reference	0.99723 ± 0.00006	-277	195	8
RAPID (Radially Detailed)	0.99701	-299	2	1
RAPID (Full FM)	1.00151	+151	31	1

Table 7.3: k_{eff} Results for Benchmark Problem 2

7.3.2 Axial Collapsing Exploration

Axial collapsing greatly speeds up the RAPID eigenvalue calculation by reducing the size of the fission matrix from $N * N$ to $\frac{N}{2} * \frac{N}{2}$. While this capability is already integrated into the current version of RAPID, a separate collapsing algorithm was needed to collapse the fission matrix for this particular benchmark problem. Starting with the 36 axial levels used in the model, the collapsing algorithm combined adjacent tally and source locations to obtain a collapsed coefficient value. To compare with Serpent, the same method was used, taking the calculated fission density and adding the adjacent axial locations together. Comparisons were made by re-running the RAPID model with the new fission matrix, and recording k_{eff} and fission density. A relative difference was taken between the axial fission density sums of the collapsed RAPID and Serpent models. Figure 7.6 shows a loss of information in the model due to repeated collapsing, resulting in the increase in % difference in fission. The full model shows a peak relative difference in fission near the boundary axial levels, with a value around 1%. But, if collapsing continues down to 9 axial levels, the relative difference increases to roughly 9%.

An important point here is that as the model is collapsed, the RAPID calculated k_{eff} actually drops down closer to the experimental value. The data in table 7.4 shows the difference in k_{eff} relative to the uncollapsed model, not the experimental

benchmark value.

Model	k_{eff}	$\Delta k_{eff} * 10^5$	Time (min.)	# Cores
Uncollapsed (36 levels)	1.00151	–	31	1
18 Levels	1.00104	-47	5	1
9 Levels	0.99824	-327	1.25	1

Table 7.4: Collapsed Model Comparisons for Benchmark Problem 2

From the results shown in the table above, it is clear that higher calculation speeds are inversely related to the precision of the result.

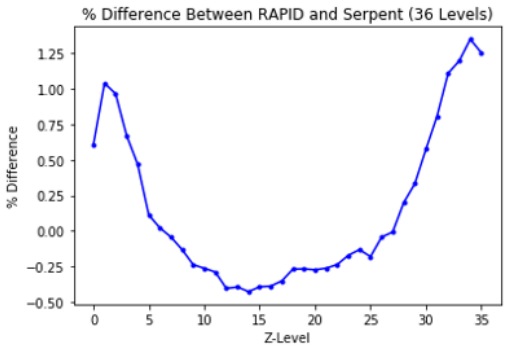

(a) Uncollapsed Difference

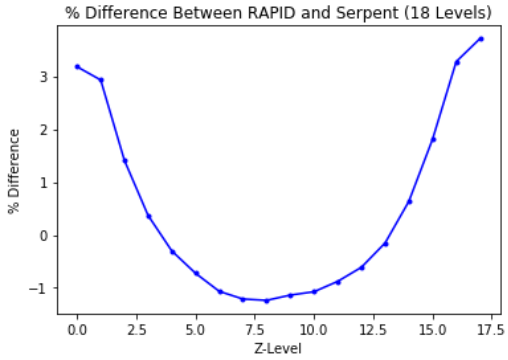

(b) 18 Axial Levels

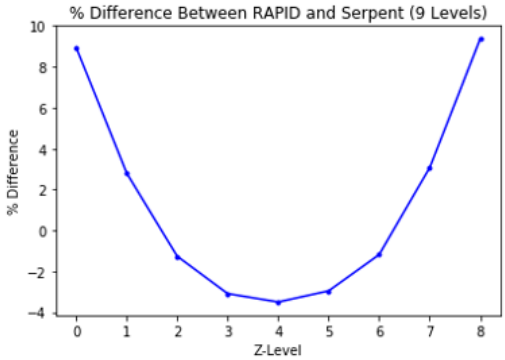

(c) 9 Axial Levels

Figure 7.6: Axial Fission Comparisons between Serpent and RAPID (Collapsed)

Chapter 8

Benchmark Problem 3

8.1 Serpent Reference Calculation

8.1.1 Model Description

This was a critical moderator height experiment, rather than a critical approach experiment like the previous two. The benchmark problem includes four assemblies, with each assembly consisting of 324 (18x18) UO_2 fuel rods, with a 1.6 cm pitch, surrounded by a stainless steel canister with a 0.05 cm cadmium slice contained within. The assemblies and the 2 cm gap between the canisters were flooded with water up to the critical moderator height of 50.11 cm into the active fuel region. This meant that 39.89 cm of the active fuel region was left exposed to air. The fuel rod pitch was 1.6 cm. Additionally, two of the corner rod locations in each assembly were replaced with stainless steel tie rods. The benchmark model called for removal of all structural materials above the critical water line except for the fuel rods and absorbing canisters. Figure 8.1 gives detailed diagrams of the benchmark geometry, as well as a schematic of the absorbing canister. The cadmium is a very strong

absorber, which leads to some issues of convergence in FM coefficient calculations.

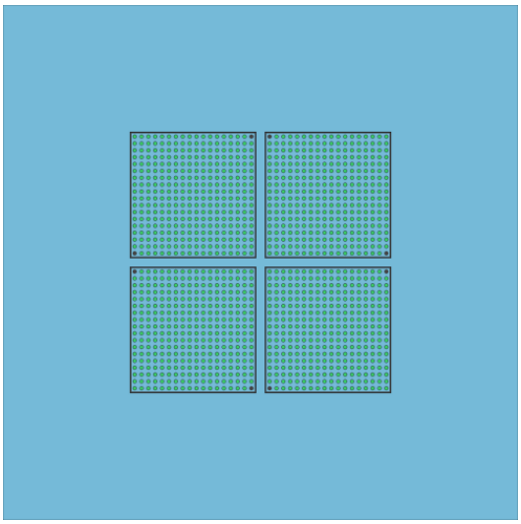

(a) X-Y View

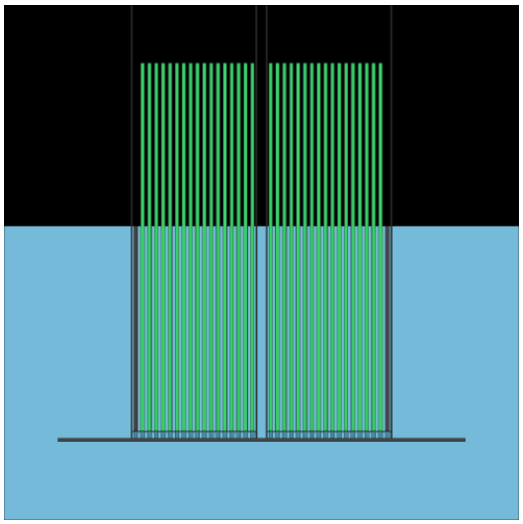

(b) X-Z View

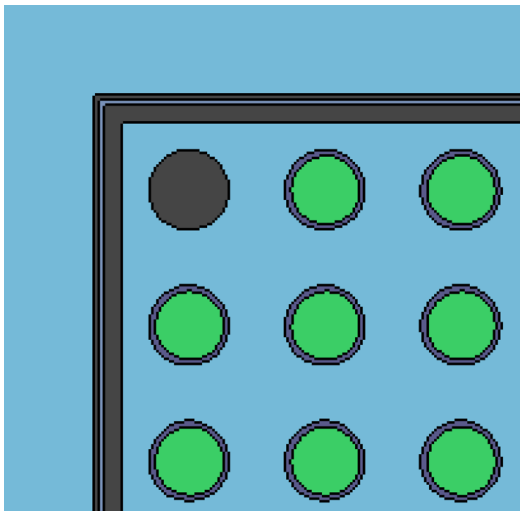

(c) Corner View

Figure 8.1: Serpent Geometry for Benchmark Problem 3

8.1.2 Serpent Reference Calculation Results

The reference experimental eigenvalue for this model is $k_{eff} = 1.00000 \pm 0.00470$. The review document provides a benchmark model written using quarter symmetry, which makes sense given the four assembly geometry. However, in the case of coefficient calculations, this geometry is not usable for this purpose as the source locations themselves would be reflected. A full geometry was needed in order to successfully run RAPID calculations for this model. Both were created, each run with 10^6 particles, 350 active cycles, and 100 skipped cycles. Both models are acceptable in matching the benchmark k_{eff} value, and the full model is acceptable for use in RAPID FM coefficient generation. The results are shown in table 8.1.

Model	Particles/Region	$k_{eff} \pm 1\sigma$	Rel. Diff. (pcm)	Time (min.)	# Cores
Experiment	–	1.00000 ± 0.00470	–	–	–
Serpent (Quarter)	21.43	1.00319 ± 0.00005	+319	372	8
Serpent (Full)	21.43	1.00314 ± 0.00005	+314	274	8

Table 8.1: Initial Serpent Results for Benchmark Problem 3

The axial fission distribution is shown in figure 8.2, showing that 99.9% of the total fission density of the system encompassing the "fuel-in-water" region and about 5 cm of the adjacent "fuel-in-air" region. This figure gives a good visual of the exponential drop-off in fission density once the fuel reaches the air region above the critical moderator height. Fission density and its associated uncertainty are shown in figure 8.3. One observation in this figure is the increase in fission density uncertainty near the edges of the assemblies due to the strong absorbing canisters.

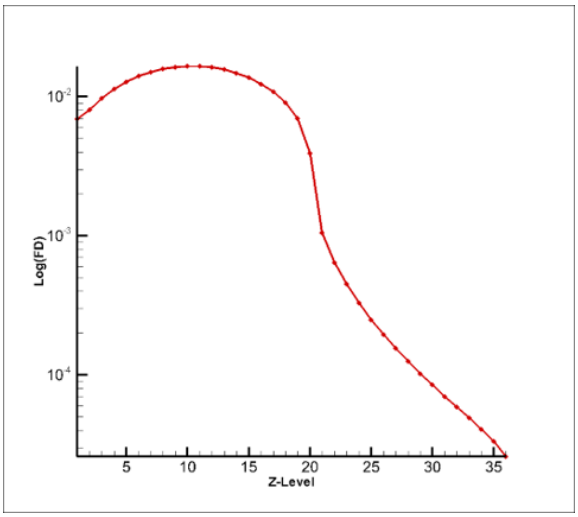

Figure 8.2: Log of Fission Density vs. Axial Level

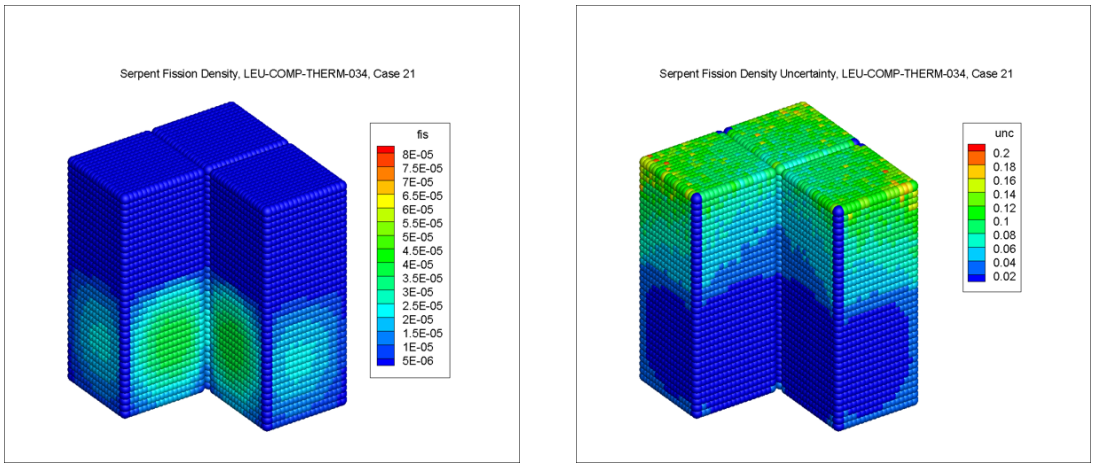

Figure 8.3: Serpent Fission Density and Uncertainty for Benchmark Problem 3

8.2 RAPID Results

The clear choice of FM coefficient generation scheme for this model was quarter symmetry. An initial set of FM coefficients was generated using 36 axial levels, with evenly distributed axial bins. However, as shown in figure 8.2, over 99% of the total fission density in the model was contained in the first 21 of those 36 axial levels, meaning the FM coefficients in the remaining 15 axial levels provided very little information. The initial eigenvalue result from RAPID severely underestimated k_{eff}. An example coefficient plot is shown in figure 8.4a and the associated uncertainty is shown in figure 8.4b. Note that the fission density distribution shows significant uncertainties in the range of about 10-15%. This high level of uncertainty in significant regions, paired with the underestimation on k_{eff} led to the conclusion that this initial set of FM coefficients was not fully converged.

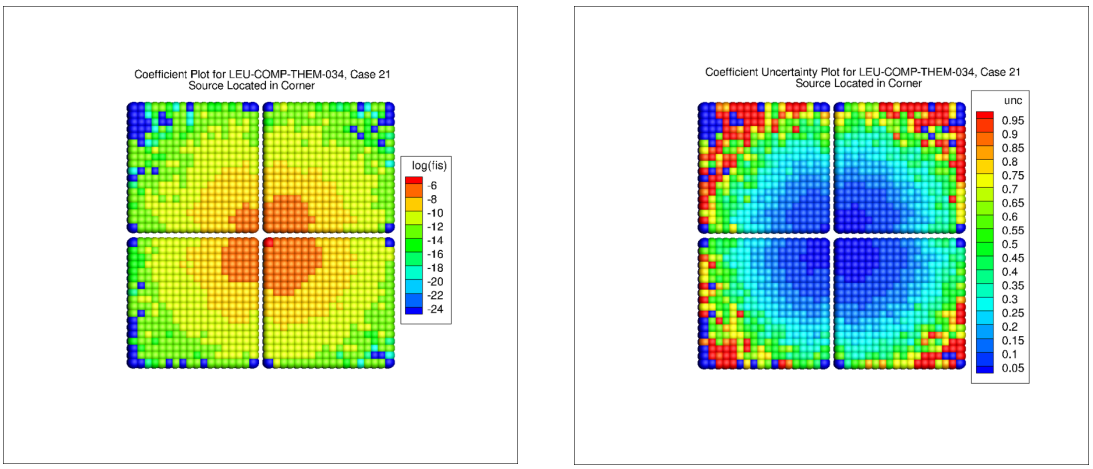

(a) FM Coefficient Plot

(b) Uncertainty

Figure 8.4: FM Coefficient Plot and Uncertainty for Benchmark Problem 3

A re-run of coefficients for this model was done, increasing the number of neutrons per FM coefficient calculation as shown in table 8.2.

Figure 8.5 shows the relative difference in fission density as calculated by RAPID,

Model	$k_{eff} \pm 1\sigma$	Rel. Diff. (pcm)	Time (min.)	# Cores
Experiment	1.00000 ± 0.00470	–	–	–
Serpent (Full)	1.00314 ± 0.00005	+314	274	8
RAPID (10^6)	0.98752	-1248	54	1
RAPID ($4 * 10^6$)	0.98589	-1411	54	1

Table 8.2: Comparison of RAPID Runs for Benchmark Problem 3

comparing the two sets of FM coefficients. Shown this figure is a large difference in the fission density distribution. Pairing this with the fact that the RAPID calculated k_{eff} dropped by 163 pcm shows that the first set of FM coefficients was indeed not converged. The reasoning behind the large underestimation on k_{eff} is discussed in section 8.3.

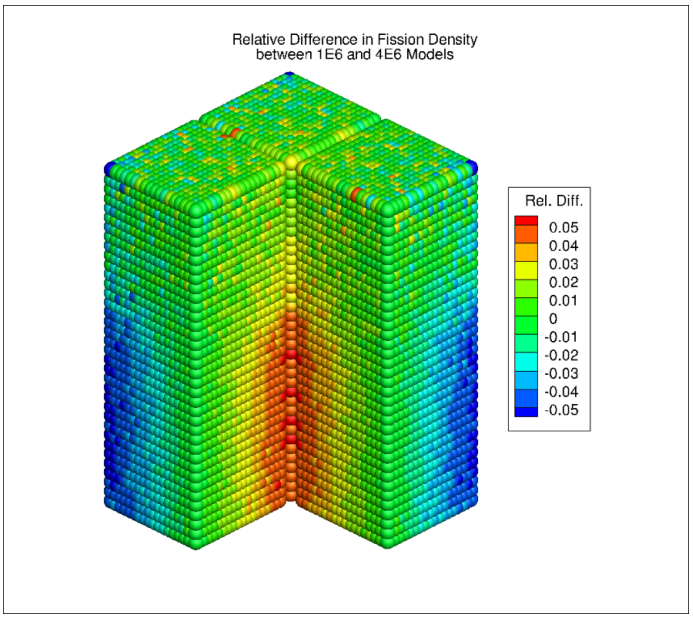

Figure 8.5: Relative Difference in Fission Density, $4E6$ vs. $1E6$ Particles

8.3 Examination of Large Differences in RAPID Calculation

8.3.1 Absorber Study Using 2-D Models

The cadmium absorbing canisters make this problem particularly unique compared to the other benchmark problems. Cadmium is a highly absorbing material, with the absorption cross-section for ^{113}Cd being on the order of 10^4 barns ($1\ barn = 10^{-24} cm^2$) at thermal neutron energies [9]. The cross section data for this specific isotope is taken from the ENDF/B-VII.1 incident neutron database and shown in figure 8.6. Thus, a study was done using 2-D RAPID models to study the accuracy compared to their respective Serpent reference calculation. Figure 8.7 shows the difference in the absorbing canisters used for the 2-D models. Figure 8.7a shows the absorbing canisters are the same as in the benchmark problem, consisting of stainless steel with an embedded cadmium slice. However, figure 8.7b fills in the cadmium region with stainless steel, meant to remove the absorption effects.

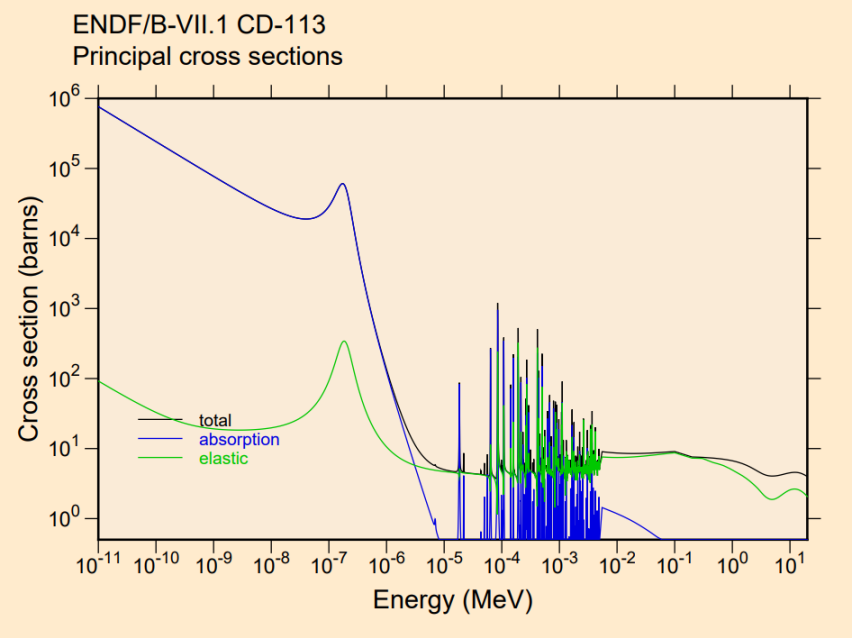

Figure 8.6: ^{113}Cd Cross-section Data

(a) Model with Cadmium (b) Model with Stainless Steel

Figure 8.7: Serpent Geometry for Benchmark Problem 3 Showing Absorber Material

A total of 324 FM coefficient calculations were necessary to build the 2-D fission matrix for these problems. This allowed for quick calculation and analysis, with

the results showing that RAPID and Serpent agreed in both k_{eff} and in fission distribution. However small the difference, RAPID underestimated k_{eff} by nearly twice as much when switching from the stainless steel canister to the stainless steel and cadmium canister. Eigenvalue comparisons are shown in table 8.3.

Model	k_{eff}	Δk_{eff} relative to Serpent
Serpent, Stainless	1.21664 ± 0.00004	–
RAPID, Stainless	1.21627	-0.00037
Serpent, Cadmium	1.08442 ± 0.00005	–
RAPID, Cadmium	1.08373	-0.00069

Table 8.3: k_{eff} Data for 2-D Calculations

The fission density plots for these 2-D models are shown in figures 8.8 and 8.9. As expected, cadmium significantly affects the fission density distribution.

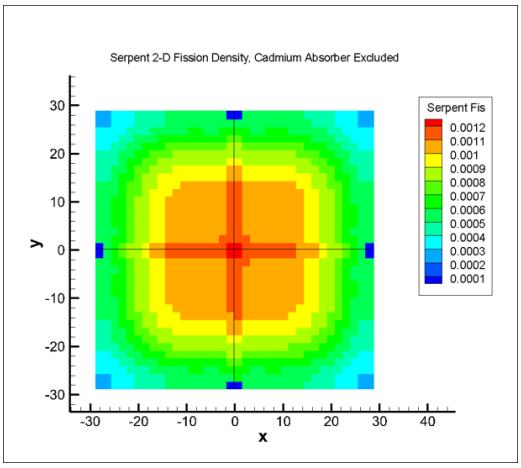

(a) Serpent Fission Density, SS

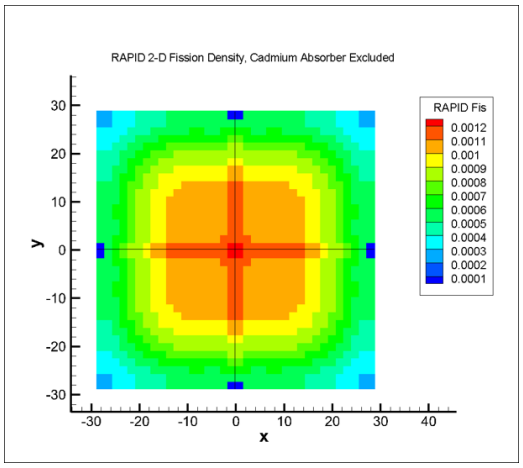

(b) RAPID Fission Density, SS

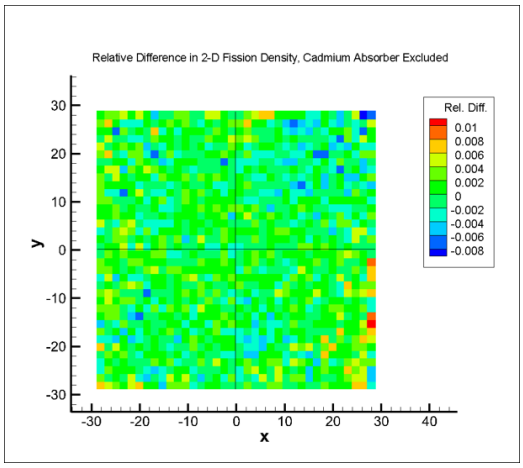

(c) Relative Difference

Figure 8.8: Fission Density Comparisons for 2-D SS Models

While the behaviors in fission are quite different between the two models, RAPID accurately calculates both the fission distribution and the eigenvalue for both systems. Because both are accurately modeled, it is shown the cadmium is not the cause of the underestimation on k_{eff}. The final aspect to examine for this benchmark problem was the axial resolution for the full calculation. For the first two benchmark problems, the axial resolution of FM coefficients had not been explored, as the results

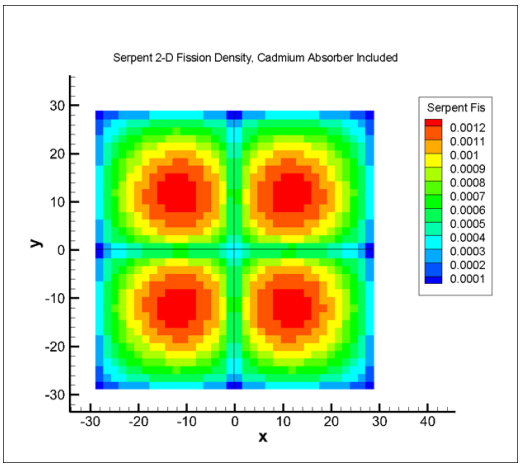

(a) Serpent Fission Density, Cd

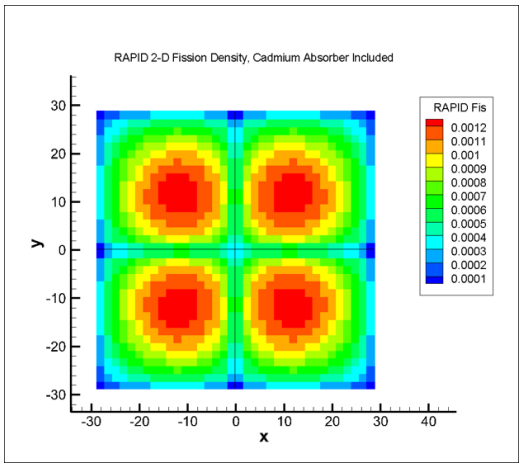

(b) RAPID Fission Density, Cd

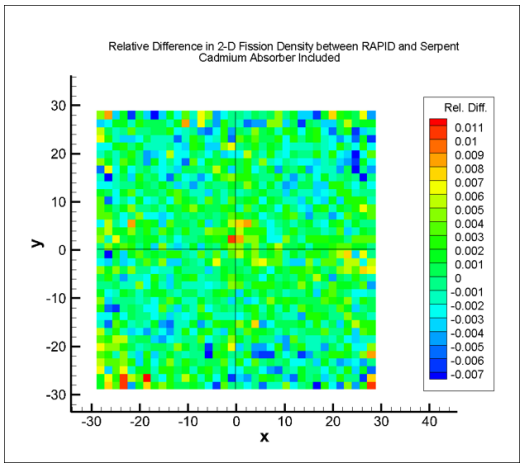

(c) Relative Difference

Figure 8.9: Fission Density Comparisons for 2-D Cd Models

were satisfactory.

8.3.2 Increased Axial Resolution for Full FM Calculation

In this section, the increase of axial resolution of tallies in the model is examined. The current axial resolution for FM coefficient calculations is 2.54 cm, or 1 inch per axial bin. For both benchmark problem 1 and 2, this resolution was sufficient in

capturing the amount of detail necessary for an accurate solution. However, this benchmark necessitated finer axial detail. The initial axial tally bin height was 2.50 cm, for a total of 36 axial levels spanning the entire length of the fuel. Since it was determined earlier that 99% of the fission was contained in the "fuel in water" region, 30 axial levels were tallied from the bottom of the fuel to the critical moderator level. The air region could have been included but would have added thousands more FM coefficient calculations for not much contribution. This brought the axial bin height down to 1.67 cm from 2.50 cm. This changed the fuel region for FM coefficient calculations such that any fuel above the critical moderator height was ignored, as depicted in figure 8.10.

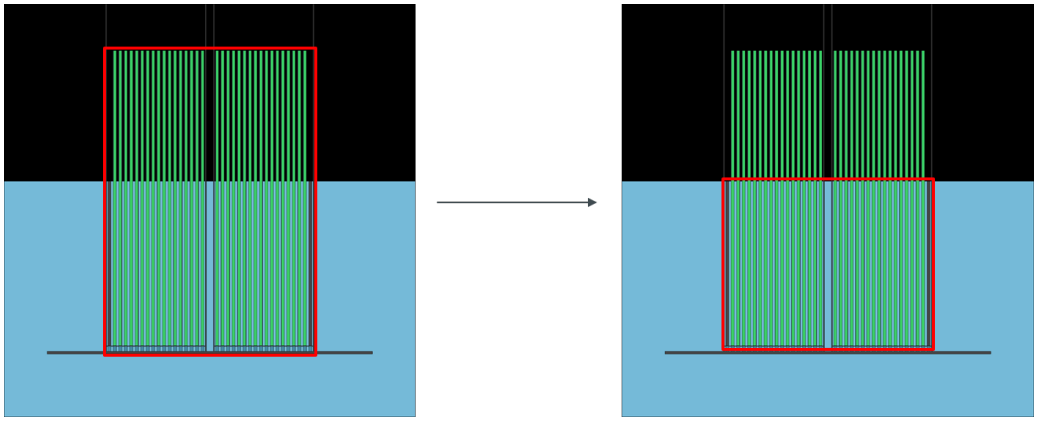

Figure 8.10: Change in Fuel Region for Increased Axial Resolution, Benchmark Problem 3

8.3.3 Eigenvalue Results Discussion

Eigenvalue comparisons are shown in table 8.4 for the experimental value, the full Serpent reference calculation, and the modified RAPID model. Shown is that both the Serpent reference model and the RAPID model fall within the experimental uncertainty defined in the benchmark problem. While the RAPID and Serpent model are not completely comparable, the increase in k_{eff} from 0.98589 to 0.99937 shows that the increased axial resolution yielded a more accurate result as it approached the experimental value of 1.0000. Due to considerations in computational resources, an emphasis on the fuel region underwater was placed as it accounts for the vast majority of fission in the model (recall figure 8.2), and an effective result could be obtained using a full FM calculation consisting of just that region. It is expected that a finer axial resolution resolves the underestimation issue, a re-run of FM coefficients including regions of fuel above the critical water line at the same axial resolution would yield a model that is more accurate.

Model	$k_{eff} \pm 1\sigma$	Rel. Diff. (pcm)	Time (min.)	# Cores
Experiment	1.00000 ± 0.00470	–	–	–
Serpent Reference	1.00314 ± 0.00005	+314	274	8
RAPID	0.98589	-1411	54	1
RAPID (Refined Axial Resolution)	0.99937	−63	45	1

Table 8.4: k_{eff} Data for Benchmark Problem 3

Chapter 9

Benchmark Problem 4

9.1 Serpent Reference Calculation

9.1.1 Model Description

Several critical core loading configurations were created using the IPEN/MB-01 research reactor which provided acceptable benchmarking problems. These provided the opportunity to model a small reactor core with a unique geometries and material compositions. The fuel itself was UO_2 fuel enriched to 4.3486 wt.% ^{235}U in a stainless steel cladding. Case 21 from the review document was modeled, and included a row of stainless steel rods and one column of copper rods in place of fuel rods. The fuel rod plugs were a combination of alumina and acrylic spacer tubes. The fuel rod schematics for this model are shown in figure 4.9. As described before, the benchmark model consists only of the various rods used in the core, the lower grid plate, and a large cylindrical column of water. Figure 9.1 shows the Serpent geometry created to benchmark specification.

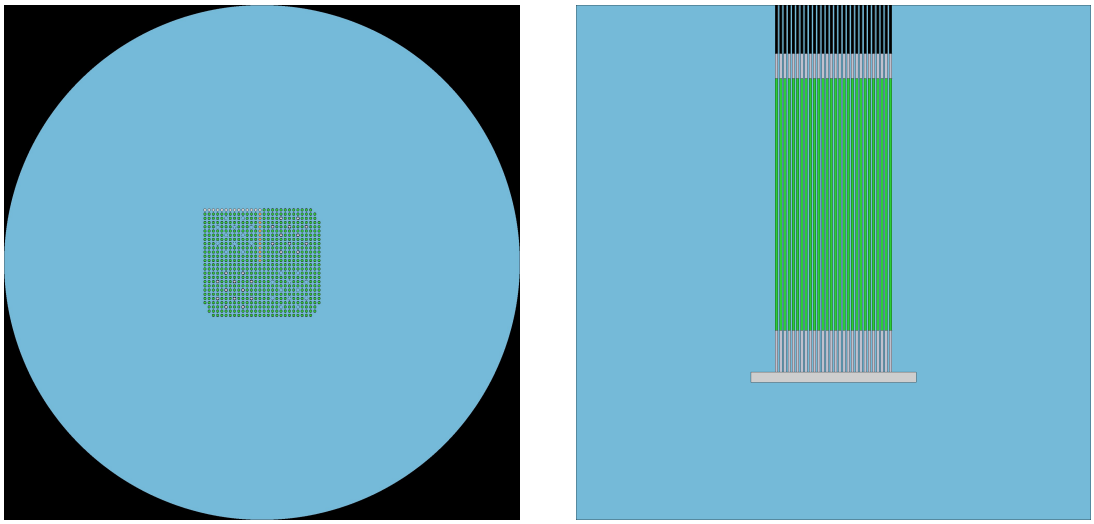

Figure 9.1: Serpent Geometry for Benchmark Problem 4

9.1.2 Serpent Reference Calculation Results

Since the experiment consisted of different critical loadings at varied temperatures, calculations are performed to provide acceptable nuclide and geometry corrections based on thermal expansion. This correction is important for this benchmark problem because there was not an appropriate thermal scattering library for the core temperature (323K). The Serpent reference calculation was run with 10^6 particles, 250 active cycles, and 100 skipped cycles. Results for the Serpent reference model are shown alongside the benchmark specification in table 9.1. The weighted fission density uncertainty was $1.19\% \pm 0.26\%$, an acceptably low level for a Serpent reference calculation. This reference calculation falls within the 1σ uncertainty and therefore is acceptable to use for RAPID FM coefficient calculations.

Figure 9.2 shows the Serpent calculated fission density and associated uncertainty. The uncertainy is small, maxing out at 1.8% in the upper back corner. In the area of increased uncertainty, the fission is a lot lower thus making it a less important region. Note that the empty corner regions were still tallied, but are just water regions. This

Model	Particles/Region	$k_{eff} \pm 1\sigma$	Time (min.)	# Cores
Experiment	–	1.00039 ± 0.00044	–	–
Serpent Reference	57.23	1.00074 ± 0.00006	257	8

Table 9.1: Serpent Reference Calculation Results for Benchmark Problem 4

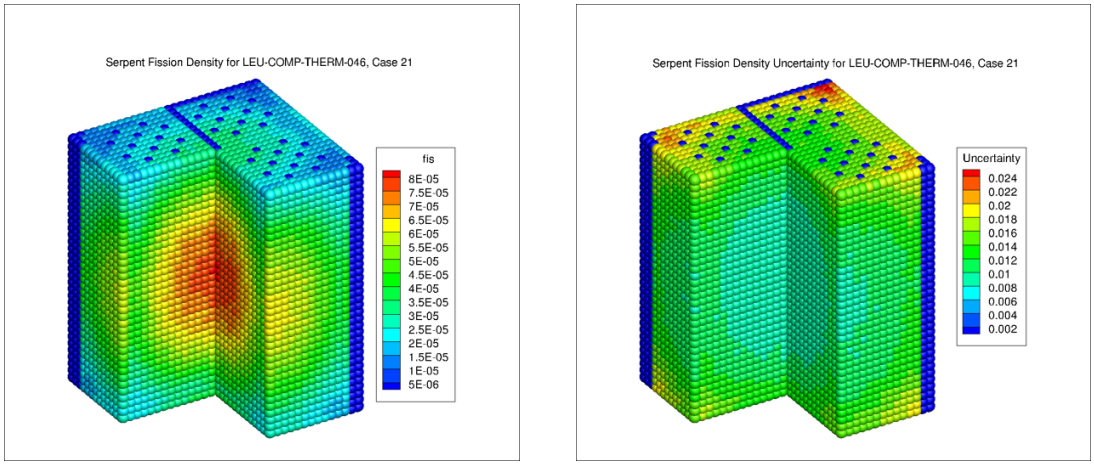

Figure 9.2: Serpent Fission Density and Uncertainty for Benchmark Problem 4

problem had the lowest experimental uncertainty by far, which is reasonable given its use as a research reactor.

9.2 RAPID Results

9.2.1 Full FM Calculation

This core geometry was not able to take advantage of any sort of symmetry, a feature different from the other three benchmark problems. To model this problem pin-wise with a sufficient axial resolution, a total of 17,472 FM coefficients were calculated. However, ignoring regions containing guide tubes, copper rods, and stainless steel rods brought this total number down to 15,408. The use of 24 axial levels led to an

Model	$k_{eff} \pm 1\sigma$	Rel. Diff. (pcm)	Time (min.)	# Cores
Experiment	1.00039 ± 0.00044	–	–	–
Serpent Reference	1.00074 ± 0.00006	+35	257	8
RAPID (Full FM)	0.99977	-62	8	1

Table 9.2: k_{eff} Data for Benchmark Problem 4

axial bin height of 2.285 cm. FM coefficients were run with 10^6 particles each.

9.2.2 RAPID Full FM Results

The RAPID results for this problem proved to be within close agreement to both the Serpent reference calculation and the experimental value. While the RAPID calculated eigenvalue was outside the 1σ uncertainty, 62 pcm is still a very small difference. The RAPID calculation was quick, only requiring about 8 minutes for the eigenvalue calculation. This data, compared to the Serpent reference and benchmark specification, is shown in table 9.2.

The side-by-side fission density plots and relative difference plot are shown in figure 9.4. Fission densities are largely in agreement, with a relative difference in fission density between RAPID and Serpent of about -0.22%. Figure 9.3 shows that there are large relative differences in fission density in the top two axial levels. The Ag-In-Cd control rod tips directly above the top axial level could be a culprit for the convergence issues of the fission source, but was not examined further as the magnitude of the relative differences were fairly mild. However, this change can be attributed to source convergence issues in the Serpent calculation, as the upper boundary of the model and the absorption from the control rod tips leads to under-sampling of the upper regions.

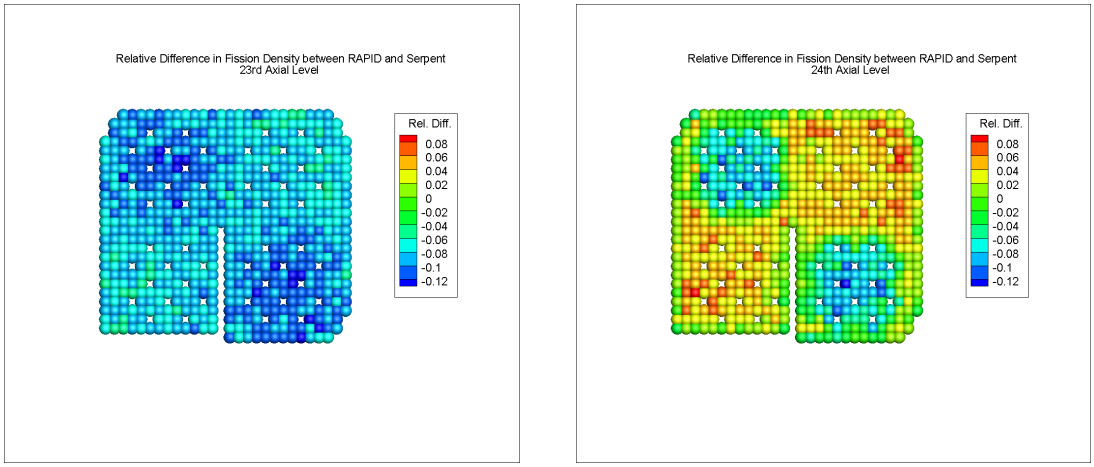

Figure 9.3: 23rd and 24th Axial Level, Rel. Diff. Plot

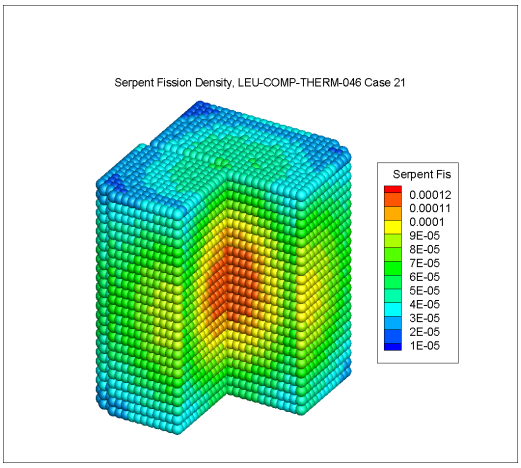

(a) Serpent Fission Density

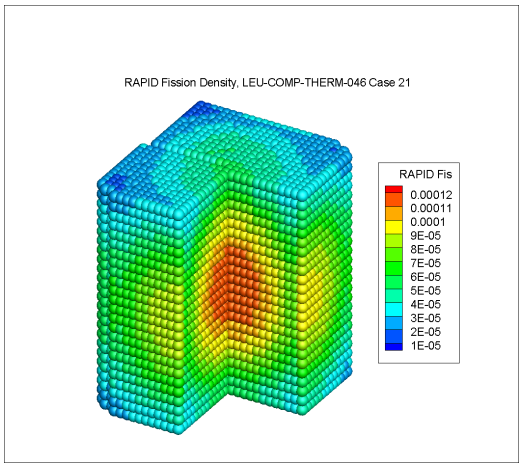

(b) RAPID Fission Density

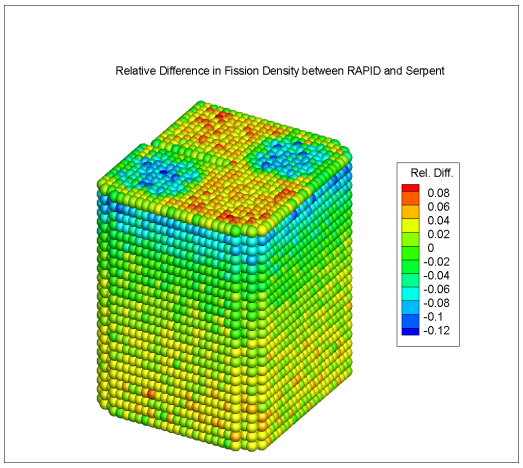

(c) Relative Difference

Figure 9.4: Fission Density Comparisons for Benchmark Problem 4

9.2.3 Uncertainty of Fission Matrix Calculations

In all of the RAPID results discussed so far, there have been no uncertainties on both the calculated eigenvalue k_{eff} and on the source which can be compared to the Serpent reference calculation. This is because uncertainties are difficult to calculate because of the amount of calculations needed is particularly large. However, two methods will be described. The first method is a brute force approach, requiring

multiple sets of FM coefficients. For each separate set, the seed of RNG is changed, providing some variation in information used in the fission matrix coefficients. Given enough trials, the sample standard deviation can be calculated for both the estimates of k_{eff} and the fission source.

The second method only involves one set of FM coefficients. After an eigenvalue calculation is performed, that information is stored and every value in the fission matrix is re-sampled using a truncated Gaussian distribution, shown in figure 9.5. A user-defined number of samples is defined and the calculation is run and re-sampled for the defined number of samples. Using this compilation of results, an estimate of the uncertainty on both k_{eff} and the source can be obtained.

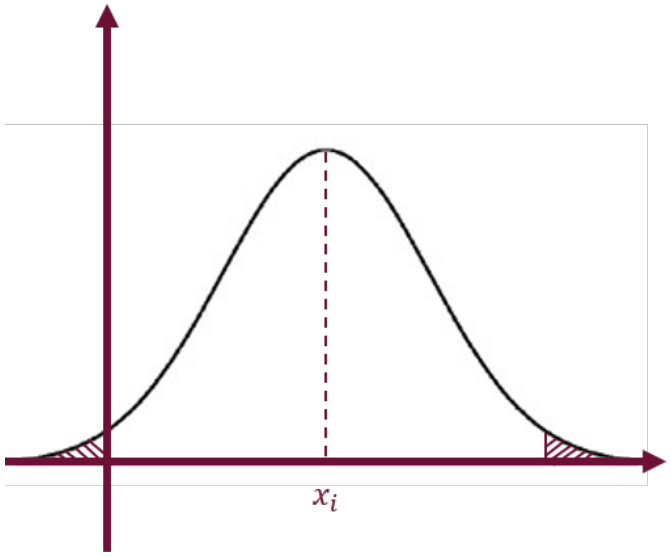

Figure 9.5: Truncated Gaussian used for Re-sampling of FM Coefficients

Uncertainties on k_{eff} and the source were determined for benchmark problem 4 using the second method. This problem was chosen because of its low eigenvalue calculation time. A total of 144 fission matrices were calculated using this re-sampling technique, which was integrated into RAPID by Valerio Mascolino. Results in table 9.3 show that RAPID's uncertainties are much smaller than the Serpent uncertainties.

Model	Uncertainty on k_{eff} (pcm)	Wgtd. Rel. Uncertainty on Fission Density (%)
Serpent Reference	0.00006	1.19%
RAPID Full Calculation	0.00001	0.13%

Table 9.3: Uncertainty Comparisons between RAPID and Serpent

Chapter 10

Conclusions and Future Work

In this thesis, four benchmark problems defined in the ICSBEP handbook were examined. They were all problems unique in geometry, offering little to no geometric symmetry. It was demonstrated that the geometric similarity, symmetry and axial translation techniques RAPID takes advantage of in large systems to drastically reduce computation time are not applicable in the modeling of these small benchmark problems. Detailed, accurate results were able to be obtained using a full fission matrix calculation. All of the RAPID results (eigenvalue and fission distribution) were in excellent agreement with the experimental benchmark data and the Serpent predictions. The following sections summarize the results, and propose possible future work.

10.1 Compilation of Results

10.1.1 Summary of Eigenvalue Results

For all four benchmark problems studied in this thesis, all but one of the RAPID calculated eigenvalues fell within the experimental uncertainty defined in the hand-

book. The one that did not fall within the experimental uncertainty was still only 62 pcm below the experimental eigenvalue, which was the closest of the four to the benchmark specification. These results are summarized in table 10.1, alongside the benchmark data and Serpent predictions.

Benchmark Problem	Model	$k_{eff} \pm 1\sigma$	Rel. Diff. (pcm)	Time (mins.)
1	Experiment	0.99980 ± 0.00310	–	–
1	Serpent Reference	0.99821 ± 0.00005	-159	491 (8 cores)
1	RAPID Full FM	0.99752	-228	114 (1 core)
2	Experiment	1.00000 ± 0.00180	–	–
2	Serpent Reference	1.00176 ± 0.00005	+176	262 (8 cores)
2	RAPID Full FM	1.00151	+151	31 (1 core)
3	Experiment	1.00000 ± 0.00470	–	–
3	Serpent Reference	1.00314 ± 0.00005	+314	274 (8 cores)
3	RAPID Full FM*	0.99937	-63	45 (1 core)
4	Experiment	1.00039 ± 0.00044	–	–
4	Serpent Reference	1.00074 ± 0.00006	+35	257 (8 cores)
4	RAPID Full FM	0.99977	-62	8 (1 core)

Table 10.1: Eigenvalue Results for Each Benchmark Problem

* see section 8.3.3 for comparability of this model.

10.1.2 Summary of Calculation Times

While speedup was not the goal of this thesis, it should still be mentioned. Eigenvalue calculation times for each of the four benchmark problems were significantly faster than their Serpent reference calculation. The calculation times for RAPID calculations and their Serpent reference calculations are shown in table 10.2. Also included in this table is the speed-up of the eigenvalue calculation. Note that all Serpent reference calculations were run using 8 cores, while the RAPID calculation

only requires 1 core.

Benchmark Problem	Serpent Time	RAPID Time	Speed-up
1	491	114	4.3
2	262	31	8.5
3	274	45	6.1
4	257	8	34.4

Table 10.2: Calculation Times and Speed-ups for Each Benchmark Problem

It should be noted that while the eigenvalue calculation times themselves are quite fast, the pre-calculation times for these benchmark problems were quite large, requiring several thousand FM coefficient pre-calculations for each benchmark problem. Table 10.3 shows the summary of pre-calculation times for this thesis, including number of FM coefficients needed for each benchmark problem. Wall clock time represents how fast each set of FM coefficients actually took. Each FM coefficient calculation was run using 8 cores, on a 56 core computing cluster.

Benchmark Problem	# FM Coefficients	NPS	Total CPU Time (Hours)	Wall Clock Time (Hours)
1	7,560	10^6	122.8	17.5
2	20,736	10^6	292.4	41.8
3	11,664	$4 * 10^6$	493.8	70.5
4	17,472	10^6	264.9	37.8

Table 10.3: Summary of FM Coefficient Pre-calculation Times

10.2 Future Work

Further studies into small and unique systems like the benchmark problems discussed in this thesis would be quite useful. Benchmarking the bRAPID burnup code using similar benchmarking problems would be useful to the continued development

of the pRAPID utility code. As only LEU fuel systems were examined in this thesis, benchmark problems using increased fuel enrichment could be studied, as the ICSBEP handbook provides benchmark problems in the moderate-to-high levels of fuel enrichment. The source code changes made to RAPID and pRAPID are now well suited for the benchmarking and modeling of small, generalized rectangular geometries. Further benchmarking efforts using the unique problems posed in the ICSBEP handbook could provide further insight into the effectiveness of the RAPID eigenvalue algorithm.

Bibliography

[1] Nuclear Energy Agency. *ICSBEP Handbook 2018*. Tech. rep. Nuclear Energy Agency, 2018.

[2] Nuclear Energy Agency. *ICSBEP Working Group Web Page*. `https://www.oecd-nea.org/science/wpncs/icsbep/`. Accessed: 2019-07-31.

[3] Forrest B. Brown. *"K-effective of the World" and Other Concerns for Monte Carlo Eigenvalue Calculations*. Conference Presentation. Supercomputing in Nuclear Applications and Monte Carlo, 2010.

[4] Alireza Haghighat. *Monte Carlo Methods for Particle Transport*. Boca Raton, Florida: CRC Press, Taylor and Francis Group, 2015. ISBN: 9781466592537.

[5] Jaako Leppänen. "The Serpent Monte Carlo Code: Status, development and applications in 2013." In: *Annals of Nuclear Energy* 82 (2015), pp. 142–150.

[6] E. E. Lewis and W.F. Miller. *Computational Methods of Neutron Transport*. 555 N. Kensington Avenue, La Grange Park, Illinois 60525 USA: American Nuclear Society, 1993. ISBN: 0894484524.

[7] Valerio Mascolino, Alireza Haghighat, and Nathan Roskoff. "Evaluation of RAPID for a UNF Cask Benchmark Problem". In: *EPJ Web of Conferences* 153 (2017).

[8] Valerio Mascolino, Nathan Roskoff, and Alireza Haghighat. "Benchmarking of the RAPID Code System using the GBC-32 Cask with Variable Burnups". In: PHYSOR. 2018.

[9] Said F. Mughabghab. *ENDF/B-VII.1 Material 4846 Evaluation*. Tech. rep. Brookhaven National Laboratory, 2010.

[10] Nathan Roskoff. "Development of a Novel Fuel Burnup Methodology and Algorithm in RAPID and its Benchmarking and Automation". PhD thesis. Virginia Polytechnic Institute and State University, 2018.

[11] Nathan Roskoff and William Walters. *RAPID User Manual*.

[12] William Walters, Nathan Roskoff, and Alireza Haghighat. "The RAPID Precalculated Fission Matrix Methodology". In: *Nuclear Science and Engineering* (2018).

[13] C.J. Werner. *MCNP Users Manual, Code Version 6.2*. Tech. rep. Los Alamos National Laboratory, 2017.

[14] G.E. Whitesides. "Difficulty in Computing the k-effective of the World". In: *Transactions of the American Nuclear Society* 14 (1971).

Appendix A

Source Code Changes

A.1 Processing Code *pRAPID.py*

The standard pre- and post-processing code our research group utilizes is a Python script which, given the desired Serpent geometry files, will automate the preparation, submission, and post-processing of FM coefficient calculations. It was written by Dr. Nathan Roskoff for use in his work developing the bRAPID algorithm [10], where the file management can get hectic. While this code initially only gave the option of using octal symmetry in coefficient file generation, it has since been generalized to handle rectangular assembly geometries, which enables the modeling of the benchmark models examined in this thesis, as well as boiling water reactor (BWR) fuel assemblies, where octal symmetry is not valid. The initial framework of the pRAPID processing code and subsequent generalization of the code were both extremely important to my research, particularly when full fission matrix calculations were necessary. Initial changes made to it were introducing a flag variable, *xy-mode*, which in essence switched off the octal symmetry in the coefficient file creation to just iterate over a specified rectangular geometry. It was further modified with another

flag to generate coefficient files to fill a whole fission matrix when necessary.

A.1.1 rdserp.f90

This is the Fortran 90 script written for use within pRAPID's post-processing section. Essentially, pRAPID filters through all the tally files and simplifies them down to a more usable format. From there, the *rdserp.f90* file is called to process and fill the fission matrix from the FM coefficient data. This code can be changed to the users liking to work with different geometries. While the initial version was meant for octal symmetry, it was rewritten on a case-by-case basis. For each benchmark problem, this script was modified to write a whole fission matrix or map into a fission matrix via quarter symmetry. At the same time, the fission matrix can be read by axial source level to be sent to another processing code which collapses the fission matrix data. A potential fix to re-writing this script for each problem would be to keep a few variations (processing for different symmetry types) involving different cases and adding a parameter in the input file to point to the correct variation.

A.2 RAPID Source Code

RAPID was initially designed to be a super fast, fission matrix-based code for solving for the criticality eigenvalue k_{eff}, sub-critical multiplication factor M, and for the fission distribution. The sheer number of FM coefficient calculations required for a full fission matrix of any modest size would lead any scientist away from selecting this method when Monte Carlo methods will do just fine. The attractiveness of using the RAPID algorithm to solve for these model values is the fact that one can cleverly take advantage of geometric similarities typically present in most commercial nuclear systems. In PWR assemblies, octal symmetry within each assembly can be leveraged. This along with mapping coefficients to the other assemblies in a given

ROI leads to a reduction in the number of FM coefficients needed by several orders of magnitude. As such, the source code was optimized to take advantage of this symmetry. As result of our group's recent work, we've been able to show that with some changes, RAPID can model geometries that cannot leverage octal symmetry, with similar levels of accuracy. Recent work includes efforts by Valerio Mascolino to benchmark the JSI TRIGA Mark II Reactor at the Jozef Stefan Institute in Slovenia, efforts by Quinn Dircks to benchmark the GBC-68 BWR fuel cask, and efforts by myself to benchmark select models from the ICSBEP handbook. The three works stated all cannot use the current octal symmetry option, with the first and last being quite small compared to commercial reactor fuel.

The changes made to the RAPID source code were similar to the changes made to the pRAPID processing code. An *xy-mode* flag was introduced to the standard RAPID input file, and "xy" versions of relevant source files were created, only being run when the flag was switched on. At the time, Quinn and I worked to add a flag to handle even numbers of fuel rods and rectangular geometries, which was sufficient to allow RAPID runs using 10x10 BWR fuel and my then current benchmark, consisting of 20x14 fuel clusters. Later on, it was found this only ran correctly when the number of fuel rods in the x-direction was greater than or equal to the number of fuel rods in the y-direction. The big issue with the RAPID source code as it stood was that it was written under the assumption that the number of fuel rods in the x-direction would always match the number of fuel rods in the y-direction, thus not requiring a variable for fuel rods in the y-direction. This necessitated the addition of xy-mode source files to properly allocate memory when the number of fuel rods in the y-direction was indeed greater than in the x-direction.

Appendix B

Codes Developed

Several utility codes were developed for use in this thesis. Scripts were written in Python 3.0 and in Fortran 90 depending on their use.

1. *benchmark_det_filter.py*

   This code was used as a general utility code to process RAPID and Serpent tally data, capabilities include:

   - Process tally data and write to output files usable by the Tecplot plotting software
   - Relative difference calculations
   - Boundary correction file creation
   - Collapsing Serpent fission density

2. *collap_sez.f90*

   Fortran script written to collapse the fission matrix axially by a factor of 2 or a factor of 4. It was used for the axially collapsing study in section 7.3.2.

3. *jrapid.f90*

   Fortran script written separate from *rdserp.f90* to combine the axial levels of the fission matrix data into the whole fission matrix.

Appendix C

Changes to pRAPID

pRAPID was heavily modified from its original form to meet the needs of the benchmark problems studied in this thesis. Many flags were added to the input file to make use of different run modes in order to append to pRAPID rather than mess with the original framework. All changes only apply to fresh fuel scenarios, as burnup was not considered by any of the benchmark problems studied.

All parameters listed are defined in the pRAPID input file, *dim.py*.

1. *proc_debug*

   Skips tally file read-in and .xyz file creation, telling pRAPID to only process files. Useful for debugging the *rdserp.f90* script when running full FM calculations as the file read-in can take up to an hour.

2. *xy_mode*

   General flag allowing for the inclusion of the X-Y mode code. This is a group of parameters incorporating the generalized rectangular geometry definitions needed for all four of my benchmark problems. This change also optimized the memory allocation of the fission matrix definition in RAPID. Table C.1 shows

the time speed-up of the standard RAPID models when the *xy-mode* flags are switched on.

Model	k_{eff}	Time	Time w/ XY Flag	Speed-up
RAPID	0.99500	3.73	1.91	1.95
RAPID w/ Boundary Corr.	1.00195	5.88	2.98	1.97

Table C.1: Speed-up for Standard Methods after Memory Optimization

3. *hella_coeffs_mode*

   General flag with three options of FM coefficient generation scheme.

   - *hella_coeffs_mode* = 0

     FM coefficients are generated for the central axial level of the central assembly only.

   - *hella_coeffs_mode* = 1

     FM coefficients are defined pinwise for every assembly, only at the central axial level.

   - *hella_coeffs_mode* = 2

     This is the option for full FM calculations, allowing for FM coefficients to be generated arbitrarily radially and axially.

4. *npxarr, npyarr*

   Variables used to define the number pins per assembly in the x and y direction.

5. *bl_pin_x, bl_pin_y*

   Geometric coordinates of the center of the bottom left fuel pin, used to initialize source location for FM coefficients.

6. *narx, nary*

   Number of fuel assemblies tallied in the x and y direction for FM coefficients.

7. *z_bins, z_bottom,z_top*

   Used to define the number of axial tally bins for FM coefficient calculations, as well as defining the start and end points.

8. *coeff_coarse, coeff_fine*

   Allows for different particle numbers to be run for different axial levels of FM coefficients to deal with regions of higher uncertainty.

9. *zf_start, zf_end*

   Used to define the axial range where the higher number of particles are run.